NASA TECHNICAL NOTE

NASA TN D-6646
c. 1

TECH LIBRARY KAFB, NM
0133173

LOAN COPY: RETI
AFWL (DOU
KIRTLAND AFB,

NASA TN D-6646

APOLLO TELESCOPE MOUNT THERMAL SYSTEMS UNIT THERMAL VACUUM TEST

by H. F. Trucks, Uwe Hueter, J. H. Wise, and F. D. Bachtel

George C. Marshall Space Flight Center
Marshall Space Flight Center, Ala. 35812

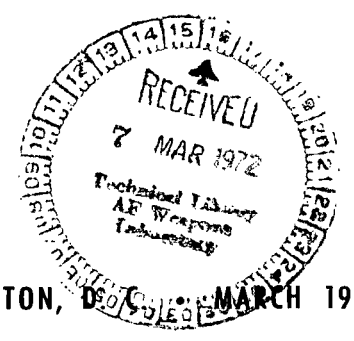

NATIONAL AERONAUTICS AND SPACE ADMINISTRATION • WASHINGTON, D. C. • MARCH 1972

TECH LIBRARY KAFB, NM
0133173

1. REPORT NO.	2. GOVERNMENT ACCESSION NO.	3. RECIPIENT'S CATALOG NO.
NASA TN D-6646		

4. TITLE AND SUBTITLE
Apollo Telescope Mount Thermal Systems Unit Thermal Vacuum Test

5. REPORT DATE
March 1972

6. PERFORMING ORGANIZATION CODE

7. AUTHOR(S)
H. F. Trucks, Uwe Hueter, J. H. Wise, and F. D. Bachtel

8. PERFORMING ORGANIZATION REPORT #
M372

9. PERFORMING ORGANIZATION NAME AND ADDRESS
George C. Marshall Space Flight Center
Marshall Space Flight Center, Alabama 35812

10. WORK UNIT NO.

11. CONTRACT OR GRANT NO.

13. TYPE OF REPORT & PERIOD COVERED
Technical Note

12. SPONSORING AGENCY NAME AND ADDRESS
National Aeronautics and Space Administration
Washington, D. C. 20546

14. SPONSORING AGENCY CODE

15. SUPPLEMENTARY NOTES

16. ABSTRACT

The Apollo Telescope Mount is a module of the Skylab Orbital Assembly which is designed to expand the knowledge of manned earth-orbital operations and accomplish scientific objectives. The Apollo Telescope Mount will be the first manned solar observatory to observe, monitor, and record the structure and behavior of the sun outside the earth's atmosphere. The Apollo Telescope Mount design also contains the Skylab pointing and attitude control system, a data and communication system, and a solar array/rechargeable battery power system.

The Apollo Telescope Mount's Thermal Systems Unit was utilized to conduct a full-scale thermal vacuum test to verify the thermal design and the analytical techniques used to develop the thermal mathematical models. This report discusses thermal vacuum test philosophy, test objectives, test configuration, test monitoring, environment simulation, vehicle test performance, and data correlation. Emphasis is placed on planning and execution of the thermal vacuum test with particular attention on problems encountered in conducting a test of this magnitude.

17. KEY WORDS	18. DISTRIBUTION STATEMENT
Thermal vacuum test Sun, structure and behavior Skylab Battery power system	

19. SECURITY CLASSIF. (of this report)	20. SECURITY CLASSIF. (of this page)	21. NO. OF PAGES	22. PRICE
Unclassified	Unclassified	74	$3.00

*For sale by the National Technical Information Service, Springfield, Virginia 22151

NOTICE

Because of a waiver initiated and signed in compliance with NASA Policy Directive (NPD) 2220.4, para. 5-b, the International System of Units of measurement has not been used in this document.

TABLE OF CONTENTS

TABLE OF CONTENTS (Concluded)

LIST OF ILLUSTRATIONS

LIST OF ILLUSTRATIONS (Concluded)

LIST OF TABLES

ACKNOWLEDGEMENTS

Throughout the Apollo Telescope Mount thermal systems unit test program, S&E-ASTN-PTA received valuable assistance from the Martin-Marietta Corporation, ATM Thermal Unit, supervised by Lawrence D. Lancaster, and the Brown Engineering Company, Inc., Thermal Engineering Section, supervised by J. J. Urbanski. In addition, all data analysis presented in this report was performed by these contractor personnel except analyses pertaining to the environmental simulation. S&E-ASTN-PTA gratefully acknowledges the valuable support of Mr. James McLane and the Space Environment Simulation Laboratory for providing overall direction of the thermal vacuum test facility.

DEFINITION OF SYMBOLS

Symbol	Definition
H α - 1	Harvard College Observatory hydrogen alpha
H α - 2	Apollo Telescope Mount hydrogen alpha
α	Infrared absorptivity
α_s	Solar absorptivity
Δ	Delta (change)
ϵ	Emissivity
σ	Stefan-Boltzmann constant
M/W	Methanol/Water

APOLLO TELESCOPE MOUNT THERMAL SYSTEMS UNIT THERMAL VACUUM TEST

INTRODUCTION

The Apollo Telescope Mount (ATM) is part of the Skylab, an earth-orbiting space station, scheduled to be launched by the National Aeronautics and Space Administration (NASA) in 1973. The Skylab (Fig. 1) includes the Saturn V Workshop, the Command Service Module (CSM), the Multiple Docking Adapter (MDA), the Airlock Module (AM), and the ATM. The Skylab programs intend to perform scientific investigations in earth orbit, to study long-duration space flight effects on men and systems, and to collect information useful for future space programs. The ATM mission objective is to observe the sun outside the earth's atmosphere. High-resolution observations of the solar disc will provide data in the visible, ultraviolet, and X-ray regions of the electromagnetic spectrum to enable better understanding of physical processes occurring on the sun.

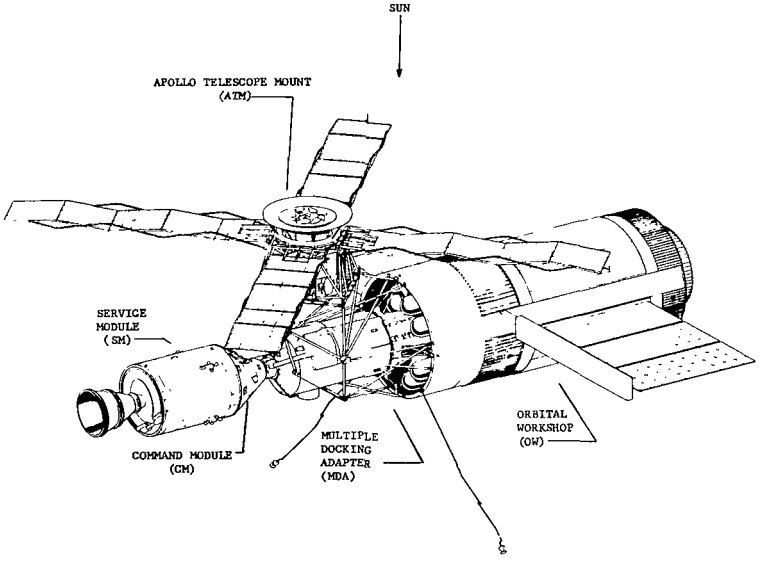

Figure 1. Skylab.

The ATM contains eight solar telescopes housed in a cylindrical canister that mounts to an octagonal rack through gimbal and roll rings. The rack structure also provides support for a sun shield, four X-shaped solar arrays, and various ATM electrical and mechanical components. Figure 2 shows the overall ATM configuration, excluding the solar arrays.

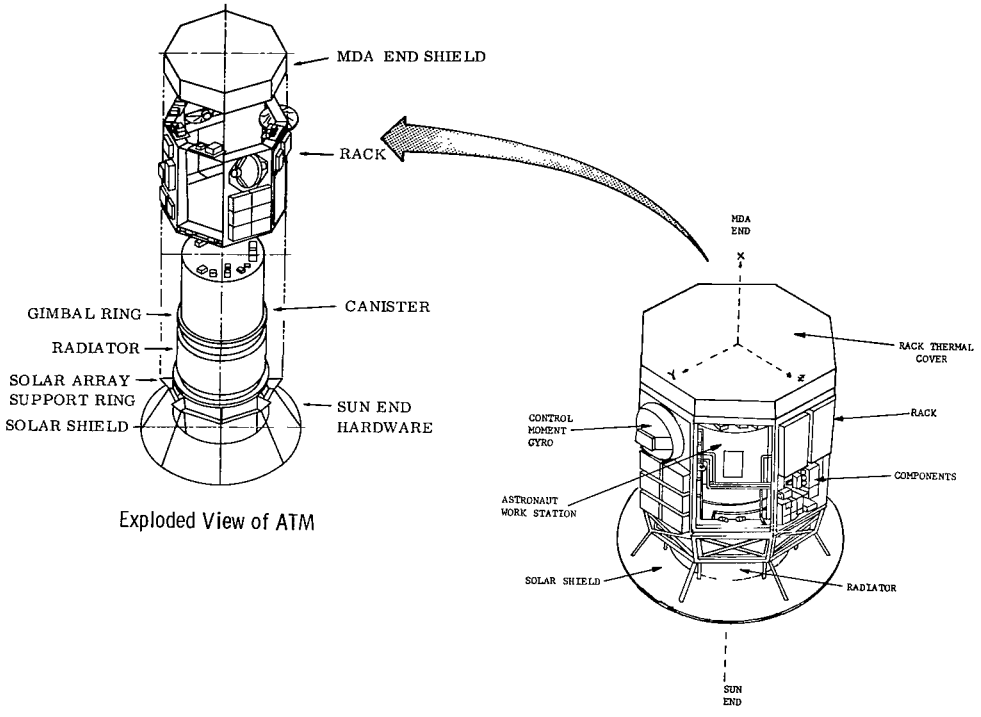

Figure 2. ATM.

To verify the thermal design prior to manufacturing a flight unit, a thermal vacuum test was planned and conducted utilizing a full-scale unit that is referred to as the ATM/Thermal Systems Unit (TSU) (Fig. 3). Most of the rack and canister components on the test article, as well as all the solar telescopes, were thermal simulators of flight hardware. However, portions of the article such as the canister active Thermal Control System (TCS), the rack and canister structure, and insulation were flight configured hardware. Also, flight hardware, such as the extravehicular activity (EVA) structure, solar arrays, and solar array support structure, was omitted from the test article; but their thermal effects, along with effects of other modules of the Skylab, were included in the environmental simulation system.

The thermal vacuum test philosophy was to provide a known environment to a known configuration, observe vehicle performance, and analytically predict this performance to verify the thermal mathematical modeling techniques. Test variables were independently altered to assure that modeling

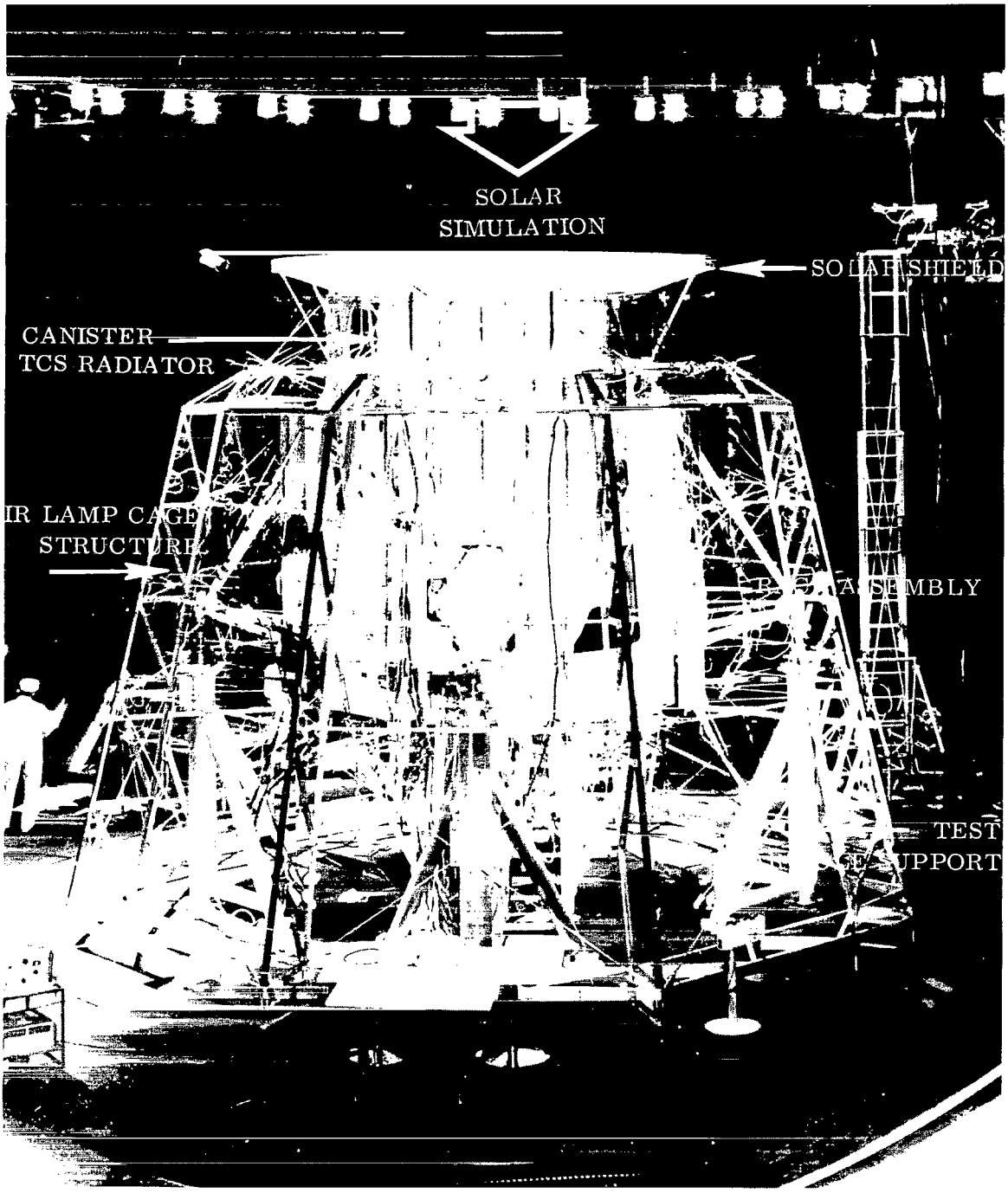

Figure 3. ATM TSU.

techniques properly simulated actual vehicle response to each variable. In addition, test environments were chosen to encompass the most severe thermal conditions expected to be encountered during the ATM mission, thereby providing, in essence, a design verification or qualification test.

The scope of this report includes detailed discussions, from a thermal analyst's viewpoint, of all aspects related to planning, executing, and analyzing the ATM TSU thermal vacuum test. In addition, emphasis is placed on test limitations, potential problem areas, and test inaccuracies that are normally encountered in large thermal vacuum test programs.

TEST PLAN

Test Philosophy

Because of the thermal design complexity and stringent telescope thermal control requirements, a decision was required early in the ATM program regarding the division of emphasis to be placed on analysis and test data. Previous experience on other programs had shown that either extreme approach was unrealistic; e. g., the Ranger program, relying heavily upon analysis, and Mariner program, primarily utilizing thermal vacuum test data. Both programs experienced flight temperatures significantly differently from the expected values. Thus, it was decided that the ATM program would utilize a comprehensive analytical approach supported by a thorough thermal vacuum test program. Final flight predictions will be obtained from detailed analytical models which are verified by thermal vacuum test data; however, limited thermal vacuum qualification testing of the flight unit will be conducted. This decision resulted from the following considerations:

1. Exact orbital environment cannot be duplicated in thermal vacuum testing because of the vacuum chamber limitations.

2. Costs prohibit thermal vacuum testing of all conditions expected during the ATM mission.

3. Failure modes and/or parametric analysis cannot be investigated extensively in thermal vacuum tests.

4. Thermal vacuum testing does not permit flexibility to incorporate late design and/or mission changes.

5. Instrumentation limitations prohibit temperature measurements of every component on large spacecrafts.

Initial analytical studies were conducted with simplified models to allow tradeoffs involving experiment requirements, mission requirements, and candidate designs which resulted in a sound design concept capable of meeting mission objectives. Chosen design concepts were incorporated into test articles to support early developmental thermal vacuum test programs utilizing full-scale portions of the ATM. Data from these tests were utilized to (1) support construction of detailed computerized analytical models, and (2) indicate design deficiencies for easier incorporation of necessary changes. The TSU test was the last of a series of thermal vacuum tests before thermal vacuum acceptance testing of the ATM prototype and flight vehicles. Since the prototype and flight ATM's will be equipped with only limited thermal instrumentation, the TSU test constitutes the prime source of detailed thermal behavior data on the fully assembled ATM. Thus, the primary objective of the TSU test program was to verify analytical techniques that were utilized to develop detailed analytical models. To achieve verification of analytical techniques, tests must be conducted with a known, analytically predictable test environment which may or may not duplicate the anticipated space environment. The requirement of providing a known environment resulted in emphasis on design, calibration, and operation of the environmental simulator discussed in subsequent sections of this report. However, by establishing known test environments which duplicate, as closely as possible, maximum and minimum anticipated flight environments; limited acceptance or qualification tests may also be performed. These tests are planned to force a design weakness (if it exists) so that the potential failure point is known as well as the type of failure. Consequently, areas where design changes are desirable can be located.

Test Objectives

Based upon the above test philosophy and consideration of the overall program, the ATM TSU thermal test objectives were established as follows:

1. Verification of thermal design and operation of the ATM when exposed to maximum and minimum thermal vacuum environmental conditions.

2. Collection of test data for verification of the analytical techniques used to construct ATM thermal models.

3. Determination of any significant thermal problems that could adversely affect the success of the ATM program in subsequent testing and flight.

4. Development of shipping, handling, and testing techniques for prototype and flight hardware.

Test Conditions and Requirements

The ATM TSU test program [1] provided a series of test conditions (Table 1) which simulated the extreme thermal environmental conditions, various mission phases, and variable internal power dissipation. These test conditions were sequentially oriented to minimize the required thermal vacuum test time; however, each test condition was carefully established to support achievement of the test objectives as discussed below.

Test Run 1 (Orbital Heating Simulator). The first chamber pumpdown was solely for calibrating the orbital heating simulator (IR cage) since the single most important test criterion was to provide a known thermal environment.

Test Run 2 (Cold Soak). The cold soak test consisted of preconditioning the test article to approximately 70°F, turning off all IR cage and test article power, and allowing the test article to cool. Thus, all power and most flux simulation uncertainties were eliminated from the test run and resulting data were utilized to verify capacitance of analytical models.

Test Run 3 (Steady State Extreme Cold/Power Off). Steady state extreme cold environments were imposed on the TSU with all test article power deactivated. This run simulated worse-case performance for a dormant storage mode. Also, test data for verification of test environment modeling techniques were obtained while suppressing two possible error sources: capacitance and component power dissipation rates.

Test Run 4 (Steady State Extreme Cold/Power On). Steady state extreme cold environments of Test Run 3 were continued; however, components, canister TCS, and telescopes' TCS were activated and the telescopes were placed in a standby mode. This test was conducted to simplify initial data correlation by enabling steady state thermal analysis to be performed that would verify power dissipation rates.

TABLE 1. ATM TSU TEST SUMMARY

	Orbital Heating Simulator Calibration	Cold Soak	Operational										Pre-operational	Activation	Ambient
			Cold Case						*Hot Case*						
	Run 1	Run 2	Run 3	Run 4	Run 5	Run 6	Run 7	Run 14	Run 8	Run 9	Run 10	Run 13	Run 11	Run 12	Launch G/C
Test Duration (hr)	70	12	53	35	12	44	10.5	6.5	42	30	8	4	7.8	20	8
Canister Telescope Power	Off	Off	Off (1)	Standby (6)	Standby (6)	Operational	Operational	Operational	Off (2)	Operational	Operational	Operational	*Off*	Off (1)	*Operational*
Canister TCS Heaters	Off	Off	Thermostatic Control	Thermostatic Control	Thermostatic Control	Thermostatic Control	Thermostatic Control	Thermostatic Control	Thermostatic Control	Thermostatic Control	Thermostatic Control	Thermostatic Control	Off	Thermostatic Control	Thermostatic Control
Canister Fluid TCS	Off	Off	Off	On	On	On	On	Off	Off	On	On	On	Off	On	Off
MDA End of Canister Electronic Components	All Off	(3)	Off	Off	All On	All On	All On	All On	All Off	All On	All On	All On	Off	All On	All On
Rack Equipment Duty Cycle	Off	Off	Off	On	On	On	On	Off	Off	On	On	On	Off/On (4)	On	On
Rack Equipment Heaters	Off	Off	Off	Thermostatic Control	Thermostatic Control	Thermostatic Control	Thermostatic Control	Off	Off	Thermostatic Control	Thermostatic Control	Thermostatic Control	Thermostatic Control	Thermostatic Control	Thermostatic Control
Orbital Heating Simulator	On	Off	Average Steady State Heat Flux; Extreme Cold Env.	Average Steady State Heat Flux; Extreme Cold Env.	Transient Orbital Heat Flux; Extreme Cold Env.	Average Steady State Heat Flux; Nominal Hot Env.	Transient Orbital Heat Flux; Nominal Hot Env.	Average Steady State Heat Flux; Extreme Hot Env.	Average Steady State Heat Flux; Extreme Hot Env.	Average Steady State Heat Flux; Extreme Hot Env.	Transient Orbital Heat Flux; Extreme Hot Env.	Transient Orbital Heat Flux; Z-Local Vertical	Transient Orbital Heat Flux; Cold Env.	Transient Orbital Heat Flux; Cold Env.	Off
Top Solar Simulator	Off	Off	On	On	Day-Night Cycle	On	On	On	On	On	On	On	On	On	Off
	Pump-down 1							Pump-down 2							

NOTES: (1) Does not include active canister rate gyros and H α Telescope vidicons which were turned on during this run.

(2) H α Telecopes zoom drive turned on for this run.

(3) Four of the 12 electronic components mounted on the MDA end of the canister were flight hardware and were on during this run. The remainder of the MDA end of the canister components were off. The flight components are: remote digital multiplexer (J) (line item number 88), remote digital multiplexer (K) (line item number 89), control distributer number 4 (line item number 156), and fluid TCS pump inverter assembly (line item number 198).

(4) All rack equipment turned on after 2 hr.

(5) H α - 2 telescope TV cameras off.

Test Run 5 (Transient Extreme Cold/Power On). Transient orbital environments were imposed; however, TSU power conditions remained as established in Test Run 4. The orbital average of this transient environment was equivalent to the Test Run 4 environment. This test simulated actual ATM operation under extreme cold orbital conditions. Correlation of test data with the analytical model under this condition provides one data point for final verification of modeling techniques.

Test Run 6 (Steady State Nominal Hot/Power On). Steady state nominal hot environments were imposed while the test article was in a full operational mode. Nominal conditions provide an indication of expected orbital operational performance while steady state test data simplify the thermal analysis.

Test Run 7 (Transient Nominal Hot/Power On). This test is a continuation of Test Run 6 with the steady state environment changed to an equivalent orbital transient environment to provide additional data for final modeling techniques verification.

Test Run 8 (Steady State Extreme Hot/Power Off). Steady state extreme hot environment was imposed on a dormant test article. This run simulated the best-case performance for a dormant storage mode as well as providing additional data for verifying test environment modeling techniques.

Test Run 9 (Steady State Extreme Hot/Power On). Test Run 8 environments were continued; however, the test article was placed in a fully operational mode to obtain additional steady state data for thermal analyses.

Test Run 10 (Transient Extreme Hot/Power On). This test run is a continuation of Test Run 9 with steady state environments changed to equivalent orbital transient environments. This test run simulated the worse-case actual ATM operational performance under extreme hot orbital condition and provided data for final verification of modeling techniques.

Test Run 11 (Pre-Operational). The test article was preconditioned to approximately 70°F to simulate anticipated launch temperatures. Then, cold transient environments simulating the first 7.8 hr of the actual mission were imposed to investigate the mission pre-operational phase. All test article equipment was dormant at test initiation. Equipment activation was planned according to actual mission constraints. Thus, after 2 hr, all rack equipment was activated.

Test Run 12 (Activation). This run is merely a continuation of Test Run 11; however, in accordance with mission constraints, the canister was activated at the start of this test run (7.8 hr after simulated launch) by applying power to the canister TCS and the telescope's TCS. Also, experiments were placed in a standby mode. This test run was terminated when thermal equilibrium was established in the canister, thereby providing an estimate of the actual activation time before obtaining solar data. This information is utilized when planning astronaut timelines.

Test Run 13 (Earth Pointing). This test run was designed to investigate ATM performance and constraints while in the earth pointing attitude required to fulfill Skylab mission objectives pertaining to earth resources.

Test Run 14 (TCS Failure). This test run was designed to investigate telescopes' performance and constraints if the canister TCS fails. This failure mode was selected for testing since a canister TCS failure would compromise all ATM experiment objectives; although, by utilizing proper constraints, the telescopes should operate within their allowable temperature range.

CONFIGURATION DESCRIPTION

Flight Vehicle

The ATM (Fig. 2) is approximately 9 by 13 feet and weighs 23 000 lb. The octagonal skeleton structure, known as the rack, supports the experiment canister and serves as a mounting structure for more than 140 components, both electrical and mechanical. Electrical energy is provided by solar cells mounted on four wings deployed in an X-shaped arrangement from the rack structure (Fig. 1). Energy available from the solar cells is stored in 18 nickel/cadmium rechargeable batteries for use during the earth shadow period. Major elements providing ATM pointing and control are Control Moment Gyros (CMG's), control computers, an acquisition sun sensor, a star tracker, rate gyros, and a fine sun sensor. These components control the Skylab attitude and point the ATM with an accuracy of ±0.2 deg pitch and yaw and ±10 arc min of roll. Fine pointing of the canister is achieved through a gimbal and roll assembly that allows a relative motion of the canister to the rack of ±2 deg in pitch and yaw and ±120 deg in roll. In flight, solar activity viewed by the telescopes is fed to a control and display console, located in the MDA, for astronaut monitoring. Using these displays and fine pointing control, the astronaut can bore-sight telescopes at solar points of interest, such as solar flares.

The canister is a 135-inch long, 86-inch diameter insulated cylinder which houses eight solar telescopes, a fine pointing control system, several supporting electronic boxes, and a fluid loop thermal control system. The eight solar experiments are:

1. High Altitude Observatory (HAO) (S-052) white light coronograph telescope.

2. American Science and Engineering (AS&E) (S-054) X-ray spectrographic telescope.

3. Harvard College Observatory (HCO-A) (S-055A) ultraviolent scanning polychromator-spectroheliometer.

4. Goddard Space Flight Center (GSFC) (S-056) X-ray telescope.

5. National Research Laboratory (NRL-A) (S-082A) extreme ultraviolet spectroheliograph.

6. NRL-B (S-082B) extreme ultraviolet spectrograph.

7. Hydrogen alpha (H-α) No. 1 telescope.

8. Hydrogen alpha (H-α) No. 2 telescope.

TSU

The ATM/TSU rack, canister, insulation systems, spar, and gimbal system are flight configurations. The various TSU components located on the rack were not flight hardware, but were simulated by Thermal-Mechanical Units (TMU's). All rack flight components were simulated for testing except the roll control panel and the strut removal motor in the Astronaut Work Station (AWS), two radiofrequency (RF) multicouplers, the solar arrays, and the EBW firing units located at various locations on the rack structure. All internally mounted telescopes and components were also simulated by TMU's. In addition to electrical heat dissipation, the telescope TMU's also simulated absorbed solar energy since motors and mechanical mechanisms used to actuate the sun end aperture covers were not included or simulated in the TSU canister. The telescope's TCS was flight designed. The liquid TCS was a modified flight system consisting of (1) a strap-on temperature sensor, (2) a reduced bypass leg pressure drop, (3) a control "dither" box,

TABLE 2. ATM TSU CANISTER INSTRUMENTATION

		TCS	Canister	Components	Misc.	Telescope								Units
						GSFC	HAO	H α-1	HCO-A	H α-2	NRL-B	AS&E	NRL-A	
Temperature		49	57	87	14	23	24	34	47	33	52	30	23	473
Pressure		11	5	NA	NA	NA	NA	NA	NA	NA	NA	NA	NA	16
Percent Quality		1	NA	NA	NA	NA	NA	NA	NA	NA	NA	NA	NA	1
Electrical Power		5	NA	4	NA	2	2	2	2	2	2	2	2	25
Heat Flux	Hy-Cal	32	NA	NA	8	NA	NA	NA	NA	NA	NA	NA	NA	40
	Cali.	192	NA	NA	NA	NA	NA	NA	NA	NA	NA	NA	NA	192
Discrete		18	NA	NA	NA	NA	NA	NA	NA	NA	NA	NA	NA	18
												TOTAL		765

(4) a special Electronic Control Assembly (ECA), and (5) a modified connecting tubing. A second pump assembly was attached between the fill and drain lines on the MDA end of the canister because of a bearing failure in the primary pump package during Test Run 1.

TSU test instrumentation [2] consisted of various types of transducers and associated wiring. Flight-type transducers were used and located at flight measurement points where possible. Additional transducers were used to complete instrumentation necessary for ATM TSU real-time and post-test analyses. Approximately 1300 test article measurements were recorded of which 1100 were displayed in real or near real-time during the test. The TSU rack assembly was instrumented with a total of 647 thermocouples. Most components had five thermocouples, one on each side and on top, all located on outside component surfaces. All thermocouples were of the unwelded junction type and were either bonded or mechanically attached to the surfaces. The unwelded junction thermocouples performed satisfactorily but are not recommended over the welded junction thermocouples. The rate gyros and charger-battery-regulator modules (CBRM's) each contained one internally located thermocouple for monitoring performance of the thermostatically controlled heaters in these TMU's. Thermocouples were also located in representative locations on the rack structure, component mounting panels, and thermal covers. Most external thermocouples were within the range of -200° to +200°F, although a few were within a range from -150° to +150°F. The ATM TSU canister instrumentation consisted of 765 measurements for six parameters: temperature, pressure, percent quantity, voltage, heat flux, and discrete functions (Table 2).

Thermal Design

The wide variation of thermal design requirements for the telescopes and equipment resulted in three distinct thermal designs. First, rack components, which generally have large operating temperature ranges, are controlled passively utilizing multilayer aluminized mylar insulation, structural isolation using titanium and fiberglass mounts, surface coatings, and component power dissipation rates. The passive thermal control is supplemented with thermostatically controlled heaters, set at the component's minimum operating or storage temperature, for those components having low power dissipation rates and/or narrow temperature limits. The passive design is cold biased to prevent hot conditions with the supplemental heaters compensating during cold conditions. Second, because of stringent telescope requirements and power limitations, an active TCS was designed to provide a constant environment for the telescopes. The TCS cold plates absorb the telescope's

dissipated heat, and a fluid loop transfers the waste energy to the radiator that rejects the energy to space. This TCS is an integral part of the canister which is isolated from the external environment with multilayer insulation. Third, each individual telescope utilizes heaters because the canister TCS cannot control the telescope cases to their required temperature tolerance of ±1°F. The design is cold-biased such that the heaters have a 30-percent duty cycle under normal operating conditions. Each system is described in detail in the following paragraphs.

Rack. Thermal control of rack components is achieved by passive and semipassive methods previously described. Approximately 140 components are mounted on the rack structure, of which 39 have supplemental heaters. The rack components dissipate approximately 3000 W. A solar shield prevents direct solar energy impingement on the rack components. All external surfaces exposed directly to the environment are painted with S-13G (white paint) having an infrared emissivity, $\epsilon = 0.9$, and an undegraded solar absorptivity, $\alpha_s = 0.2$. For identification purposes, the component mounting areas are divided into several thermal zones. Configuration similarity allows the rack zones to be separated into six groups:

1. The first group contains a full length honeycomb mounting panel with components, a honeycomb quarter panel with components, and a thermal cover. An exploded view of a typical zone is shown in Figure 4. The full length panel is isolated from the structure using titanium and fiberglass mounting brackets and multilayer insulation on the backside. Components mounted

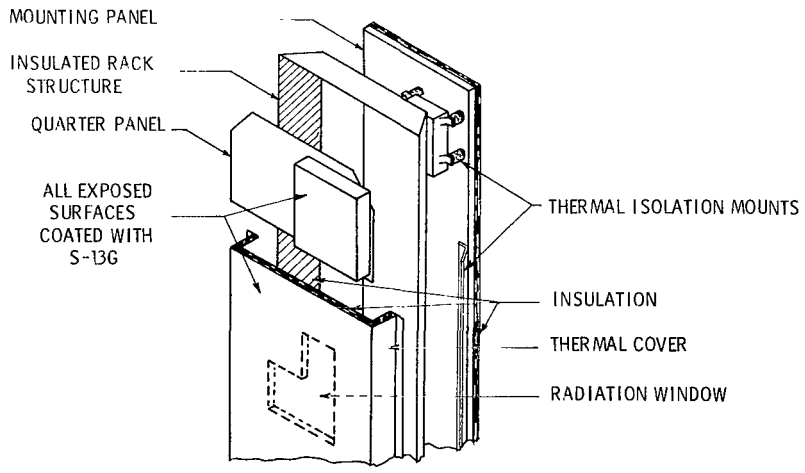

Figure 4. Typical rack zone.

on the full-length panel are completely enclosed by the mounting panel, rack structure, quarter panel, and the thermal path to thermal cover. The thermal path on the external environment is controlled by the amount of multilayer insulation added to the inside surface of the thermal cover. Boxes mounted on the quarter panels are directly exposed to the thermal environment and, in general, are high heat dissipating components.

2. The second group consists of full-length mounting panels having good thermal contact with the rack structure. The backside of the mounting panel is insulated except where six rate gyros are mounted. All components are exposed to the environment. Criteria for selecting components for this location were large boxes and/or high heat dissipation.

3. The third group contains an individually insulated Control Moment Gyro (CMG) and six CBRM's mounted on panels attached directly to the rack structure. Because of high heat dissipation rates and low maximum temperature limitations, CBRM's are exposed directly to the environment and are mounted in good thermal contact to an uninsulated mounting panel to obtain maximum heat rejection capability.

4. The fourth group is essentially an open area that provides astronaut access to the canister for film retrieval.

5. The fifth group consists of the MDA portion of the rack. Components are mounted on honeycomb shelves attached to the rack with titanium brackets. All components are covered with an insulated thermal cover.

6. The sixth group consists of the sun end of the rack. The only component in these zones is the acquisition sun sensor.

Telescope Canister. The canister's primary function is to provide a uniform and constant environment and to serve as a stable telescope mounting platform. The canister contains eight solar telescopes, four rate gyros, and a fine sun sensor. All equipment attaches to an isolated structure (referred to as the "spar") that divides the canister interior into quadrants. The telescope's arrangement is shown in Figure 5. In addition to the internal-mounted equipment, 12 electronic components are externally mounted on the end of the canister utilizing fiberglass standoffs. The TCS hardware (e. g., pumps, valves, controllers, etc.) is mounted on the canister sidewall underneath the insulation. The canister attaches to the rack by a gimbal system consisting of a gimbal ring, inner and outer gimbal bearings, and a roll ring. The canister sidewall is composed of cold plates (part of the canister TCS) that absorb

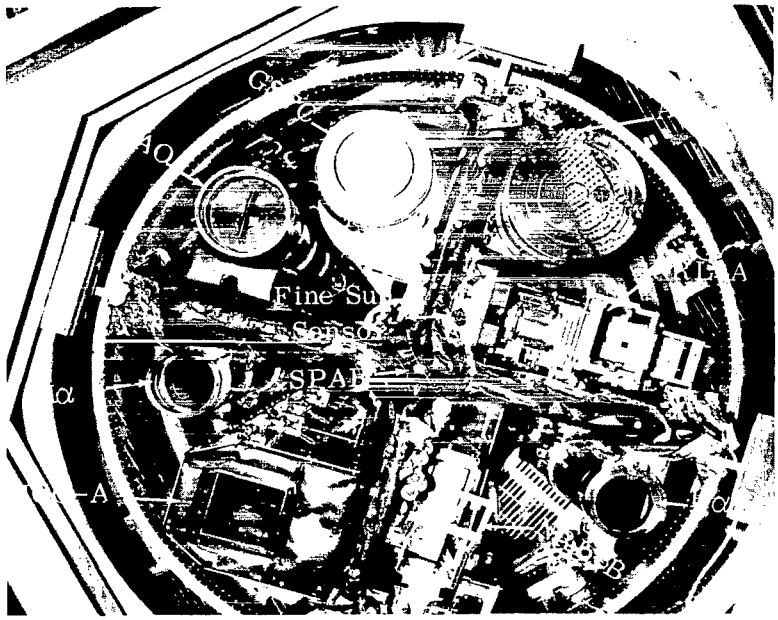

Figure 5. Telescope arrangement.

the heat dissipated by the telescopes. Interior canister walls are painted black to minimize reflections and to maximize the radiative coupling between telescopes and cold plates. The entire canister is encapsulated with multilayer aluminized mylar insulation to thermally isolate the canister interior from the external environment. The exterior insulation surface is covered with a sheet of white tedlar to protect the multilayer insulation. Four film-retrieval doors and one telescope access door are located on the canister sidewall. The canister sun end contains 10 aperture doors and 2 film-retrieval doors. In flight, the aperture doors automatically open or close whenever their respective telescope is operational or in a standby mode. The penetrations required for these doors are designed for minimum heat transfer. The sun end has an internal aluminum plate and an external fiberglass plate separated by fiberglass mounts with insulation sandwiched between the plates. The exterior surface is painted with S-13G (white) paint. The canister sun end has a 10-in. overhang to prevent solar energy impingement directly on the TCS radiator panels which are mounted on the exterior side of the sun end canister sidewall. Fiberglass standoffs, which penetrate the canister insulation, attach the radiator to the cold plate supporting structure.

The TCS is a closed-loop heat transport system that removes the heat generated by the telescopes and transports it to a radiator which rejects the heat to the external environment. Figure 6 is a schematic of the flight system. The TCS requirements are to maintain the fluid temperature entering the canister cold plates within 50±3°F and to assure that the fluid temperature rise in the canister does not exceed 5°F with a maximum telescope heat output of 500 W. The TCS consists of 16 cold plates, 4 radiator panels, a pump package, an accumulator, an inline heater, a mixing valve, associated valves, and system tubing. The working fluid is methanol/water (M/W) (80/20 percent by weight) with a nominal system flow of 850 lb/hr. As the fluid exits the pump, it is filtered and split into two parallel paths: radiator leg and heater leg. Flow proportioning through the legs is controlled by a mixing valve located at the outlet connecting point. The mixing valve is positioned by signals from an Electronic Control Assembly (ECA) which monitors the canister inlet temperature. The mixing valve normally controls the canister inlet temperature to 50°±1°F. The ECA also energizes the TCS heater when the mixed temperature drops below 47.7°F. The heater is activated in two 250-W increments at 47.7° and 47°F. Both heaters cut off at 48.5°F. The flow splits into equal flowrates before entering the cold plates and flows in parallel through the two canister halves. Each canister half has eight cold plates connected in series flow. Flow leaving the canister halves mixes and then passes an accumulator before entering the pump. In the TSU tests, the TCS was controlled by a diverting valve in lieu of a mixing valve; however, all temperature limitations were achieved. The mixing valve eliminated the instability encountered during the test.

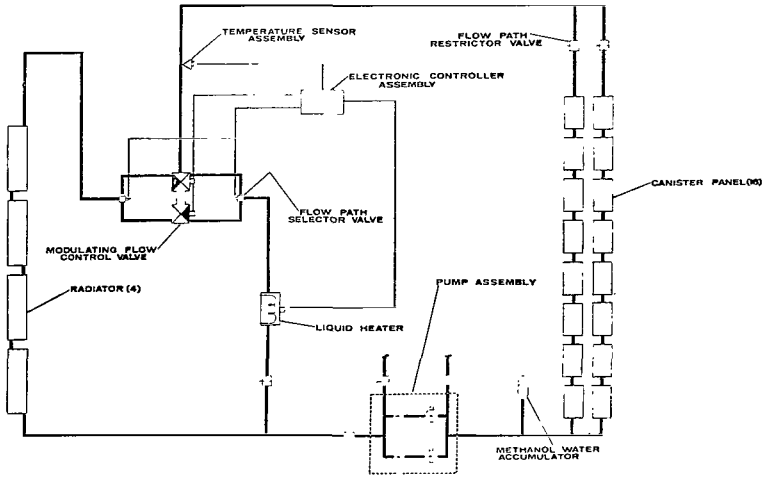

Figure 6. Canister TCS.

The spar is a cruciform aluminum structure that serves as the main support and optical bench on which telescopes are mounted. The spar is constructed of 1-in. thick aluminum plates with 2-in. diameter lightening holes. To increase the spar rigidity, spar stiffener rings are attached to each end. The spar is supported by the girth ring. Since spar temperature gradients must be minimized for correct telescope optical alignment, the spar is thermally isolated from the telescopes and spar girth ring using low conductance mounts and wrapping the entire spar with multilayer insulation. The spar insulation has an outside surface of black tedlar, $\epsilon = 0.9$, to minimize stray light and thermal reflections. This design forces radiation heat transfer to control energy exchange between the telescopes and the TCS cold plates.

Telescopes. Thermal design of the telescope assemblies must satisfy the telescope's pointing stability requirements and maintain their focal length within specified tolerances. To meet these objectives, temperature gradients in the telescopes and mounting spar must be minimized. This is achieved by minimizing heat conduction and radiation between the ATM telescopes and mounting spar while optimizing radiation heat transfer between telescope cases and cold plates. The following thermal control techniques were implemented in the telescope's thermal designs: (1) accounting for different heat dissipation rates by using thermal coatings and/or insulation as a means of controlling dissipation, (2) using high conductance material in construction of the instrument housing to reduce gradients, and (3) using thermostatic heaters to correct for thermal disturbances. Two types of heater systems being used on the telescopes are standoff heaters and integral heaters. The standoff heater concept utilizes a low capacitance thermostatically controlled radiation shield over the instrument case. Because of the low-shield capacitance, the shield temperature cycles rapidly enough that the instrument with its higher thermal capacity remains at a relatively constant temperature. These are on-off type heaters and have a fixed set point temperature. The temperature control band at the panel location is $\pm\frac{1}{2}°F$. The integral heaters surround the instrument housing and are physically attached to it. The integral heaters on the S056-GSFC experiment have an on-off type power control while the heaters on the S054 experiment use a proportional type power control. The Hα telescopes are the only passively controlled telescopes. These telescopes have a very low heat dissipation rate which allows the use of gold coating for thermal control. The low emissivity of gold coating, in effect, isolates the telescopes from external temperature variations, thus eliminating the need for an active system.

CHAMBER

The test facility was called Chamber A at the Manned Spacecraft Center, Houston, Texas. Chamber A is a stainless-steel chamber, 65 ft in diameter and 120 ft high, with a side access door 40 ft in diameter. An arrangement of the chamber with the ATM installed is shown in Figure 7. The chamber vacuum system is a combination of mechanical and diffusion pumps and a 20°K

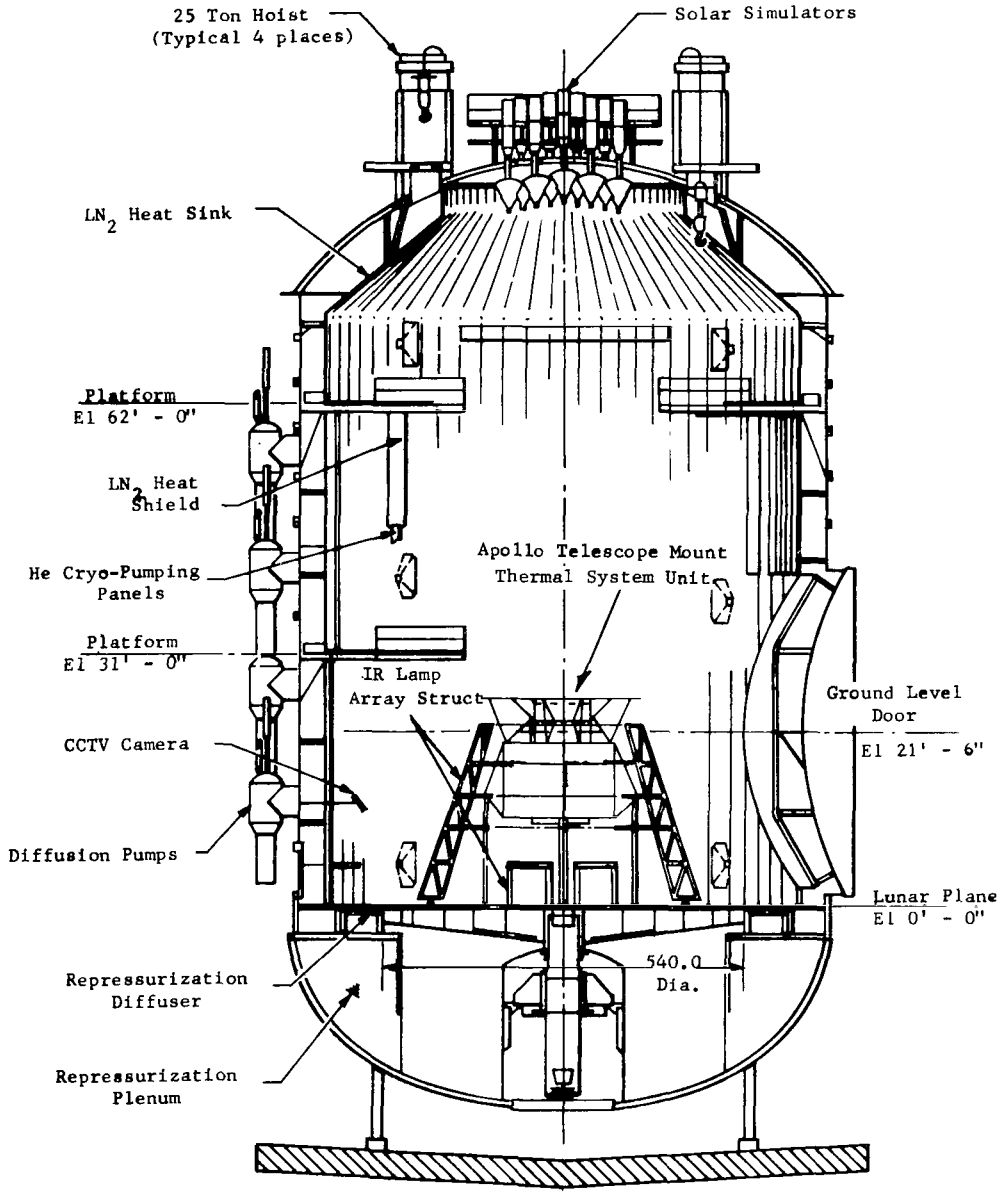

Figure 7. Test setup.

cryo-pump employing gaseous helium. The chamber can pump down to 1.0×10^{-6} torr in 20 hr. The interior of the chamber is lined with black, nitrogen cooled, heat sink panels which operate at approximately 90°K. The chamber is equipped with a top solar simulator as will be discussed later. The test facility can provide a simulated space environment of vacuum, LN_2 temperature heat sink, and solar heat flux on the upper surface of the test article. The spacecraft mounting surface in the chamber is a 45-ft diameter turntable referred to as the lunar plane. The lunar plane temperature can be controlled from 100° to 400°K by use of LN_2 cooling and stainless-steel electric resistance heaters.. The lunar plane can support a concentric load of a 150 000 lb. A more detailed description of Chamber A can be found in Reference 1.

ACE

The Acceptance Checkout Equipment (ACE) is an advanced, integrated checkout system that provides centralized, programmed control of spacecraft checkout operations. Both independent spacecraft system testing and integrated system testing are possible. Large quantities of test data can be processed and displayed in real-time, as well as recorded for later analysis, with a relatively small staff of engineering personnel.

Specifically, the ACE station performs the following functions [3]:

1. Provides the operator with controls and data processing facilities necessary to control the spacecraft test stimuli equipment.

2. Processes, displays, and records the spacecraft parameters data derived from the spacecraft ground and flight telemetry systems.

3. Provides self-check and calibration capability for itself and related equipment.

A simplified functional diagram of the system is shown in Fig. 8. The ACE system can be divided into two functional groupings: the command equipment and the data recording and display equipment. The command equipment includes the selection-to-activate-random-testing (START) modules (switching located in the control room), the uplink computer, and the Digital Test Command System (DTCS), which together form the communication path over which test commands are generated and transmitted to the spacecraft or ground support equipment (GSE). Information returning from the spacecraft or GSE is conditioned and digitized by the Digital Test Measurement System (DTMS), processed by the

Decommutation Equipment (DECOM) and the downlink computer, and recorded or displayed by various equipment in the control room. Automatic closed-loop control is achieved by linking the downlink and uplink computers through a shared memory bank. During the ATM TSU test, the system was configured to process, display, and record over 1400 real-time measurements, control approximately 150 stimuli to the spacecraft, and operate the closed-loop control system for the orbital heating simulator.

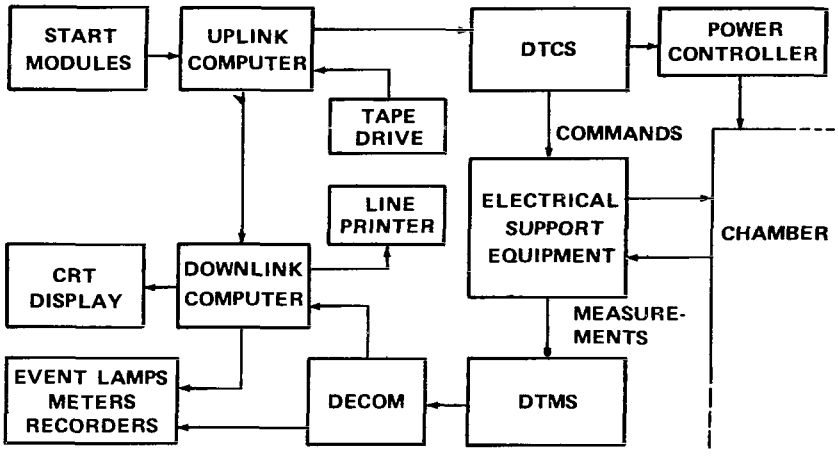

Figure 8. ACE system schematic.

Monitoring was accomplished by a combination of alphanumeric CRT displays, event lights, strip chart recorders, and real-time printouts. The CRT provided a real-time display of pertinent parameters, and event lights were used to announce various anomalies detected by the control program. Strip charts and computer printouts provided hard copy records for near real-time analysis.

Environment Simulators

Solar. The solar simulation system for Chamber A consists of 19 solar simulator modules mounted externally on top of the chamber. The simulators irradiate the vehicle through penetrations in the chamber. The solar simulation system is designed on a modular concept, with a carbon-arc system modified by an optical train, having a capability of irradiating a 13-ft diameter target at 60 to 137 W/ft^2 with a 10-percent uniformity. The solar simulator's energy distribution is composed of the following spectral percentages:

Ultraviolet	2000 to 3800 Å, approx. 8 percent
Visible	3800 to 7000 Å, approx. 41 percent
IR	7000 to 10 000 Å, approx. 23 percent
Far IR	10 000 to 20 000 Å, approx. 23 percent

All incident radiation is collimated or otherwise controlled to ensure the parallelism of the radiation to within approximately ±1.5 deg.

Orbital Heating Simulator (OHS) [4]. The function of the orbital heating simulator was to provide required transient and steady state orbital fluxes on all ATM zones other than the sun end. The fluxes were effected with a set of IR lamp arrays mounted to a skeletal structure surrounding the ATM. The lamp arrays were controlled by digital input power controllers linked to the on-site computer complex (ACE). Modified calorimeters used as heat flux sensors were mounted on each ATM zone and provided flux measurement for control and recording of the simulation. A closed-loop control system using the ACE computer was used for primary regulation of the flux. The simulator supporting structure, heating units, power controllers, heat flux sensors, and simulation control are discussed in the following paragraphs.

The supporting structure design requirements were to provide structural integrity, minimum cold wall blockage, flexible lamp mounting, and spacecraft access. Eight removable vertical sections were constructed to form a low blockage, octagonal cage with horizontal rings encircling the spacecraft. Additional framework beneath the spacecraft-supported lamps irradiating the aft end of the thermal shield. The lamps are mounted on the ends of tubular arms which project radially inward. Each arm connects to a ring with an adjustable bracket allowing the lamp to be located at any position.

RI Control Model 5236 radiant heating units featuring a tungsten filament quartz envelope lamp held in a gold-plated cylindrical reflector were used to provide the environment. The unit was selected for its low blockage, fast response, high power density, and characteristic flux profile. The profiles facilitated superposition to obtain uniform flux distributions on flat and gently curved surfaces. Lamps with 5-, 10-, and 16-in. lighted lengths provided adaptability to dimensions and geometries of various zones.

Numerical input power controllers (RI Control Model NUMERAC) regulated power to the individual lamp arrays. The NUMERAC is a solid-state power controller which accepts binary information (called counts)

directly from a computer and regulates power to the load accordingly. The controller uses a silicon-control-rectifier (SCR) circuit to selectively switch power cycles out of a 63 cycle time frame; e. g., if a binary word of 10 counts is applied, then, 10 out of every 63 cycles will be switched to the load. Selected cycles are evenly distributed throughout the time frame to lessen the flashing effect. Typical power output waveforms are shown in Figure 9. Since the controller used a 63-cycle time frame, a total of 64 different power levels (including off) could be obtained. The power level command information is stored internally by the controller and is followed until the next updating. In the event of a computer failure, the controllers would thus maintain power according to the last command received. A manual input console was included and consisted of six binary weighted switched provided manual selection of any power level from 0 to 63. A set of six pilot lights provided a readout of the selected power level, whether on manual or computer control.

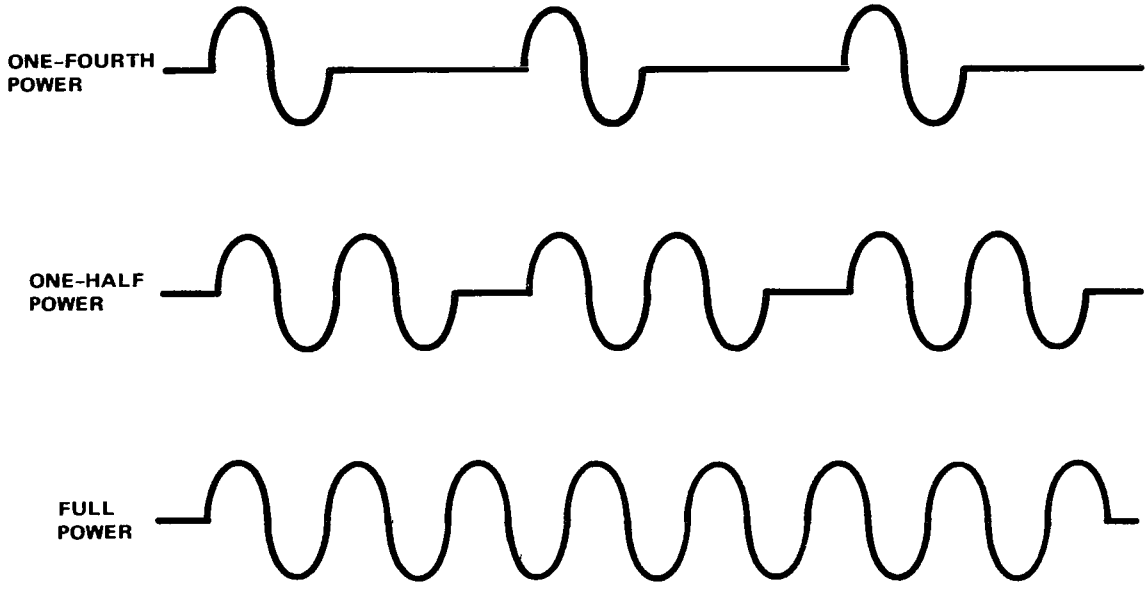

Figure 9. Typical power output waveforms.

A Hy-Cal model CCH28 bidirectional calorimeter was modified for sensing radiant heat flux. The calorimeter, a thin epoxy wafer between two metallic plates, outputs a signal directly proportional to flux passing through the wafer. Modifications included coating the sensing surface with the test article paint, embedding a thermocouple in the wafer, and bonding a copper block to the backside. With identical coatings, the sensor and test article absorb equally, thereby eliminating the need for spectral absorptivity compensation. The thermocouple measured the surface temperature for calculating

surface reradiation. The copper block heat sink negated potential errors resulting from rapid wafer temperature transients. The heat that was absorbed was measured and directly calculated as the sum of heat passing through the wafer and the heat reradiated. To facilitate removal and reuse, sensors were attached to the test article with hook and pile (Velcro) fasteners.

A closed-loop control system using a digital computer and a discrete time step was developed for primary regulation of the simulator flux. Figure 10 shows the system components. Heat flux sensors gave the feedback signal.

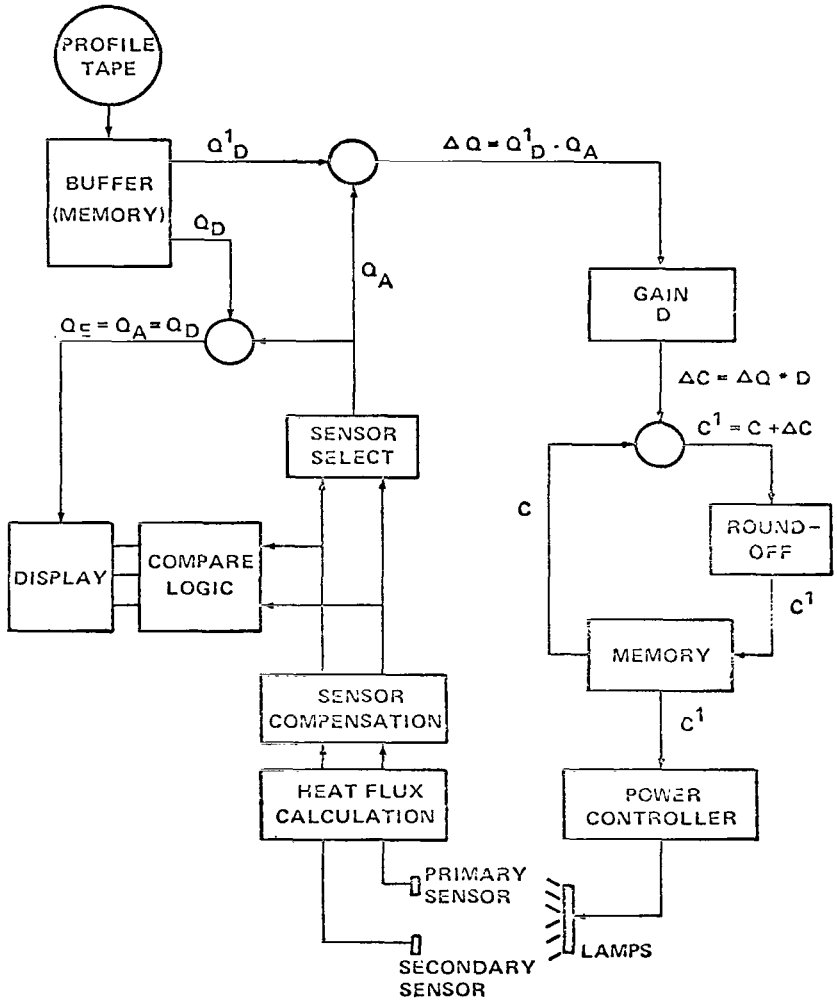

Figure 10. Orbital heating simulator control loop.

The test site data acquisition and computer facility (ACE) acquired, processed, and recorded all data, provided logic for control, displayed flux and power levels and control program conditions, and output digital commands for the required power levels. Power controllers completed the loop by converting digital commands into proportional power that was applied to the lamps. Since the system operated at discrete time steps, power was updated at regular intervals. One-min updates provided sufficient time for the sensors to react to a power increment and still maintain good temporal resolution over a 93-min orbit.

The first step in the control process is the acquisition of the actual flux level. Each zone is fitted with a primary and secondary flux sensor. Absorbed flux is calculated for both sensors and correct to average zone heat flux using a primary (H) or secondary (J) sensor correlation factor. Either sensor can control while the other serves as a monitor. Desired flux proflies, consisting of a set of values for each update interval, are stored on magnetic tape and automatically read into the memory buffer as the simulation progresses. The data are stored in files which contain the flux profiles for one orbit. A file can be repeated continuously to simulate a cyclic orbit, or several files can be chained to represent changing orbital conditions. As indicated in Figure 10, the desired flux values and the actual flux readings are compared to form the heat flux error (QE) and the delta-flux (ΔQ). QE is the difference between the actual heat flux (QA) and the desired heat flux (QD) for the interval just completed. QE indicates the simulation accuracy and is displayed. ΔQ is the difference between QA and the desired flux for the next interval (QD'). ΔQ, which represents the change necessary to achieve zero error at the end of the next interval, is multiplied by a closed-loop gain factor (D) to obtain the corrective change in counts (ΔC). This change is added to the current counts (C) to obtain the required counts for the next interval. The gain factor is determined for each zone by pretest simulator calibration, but can be adjusted during test if excessive lag or overshoot is observed. The capability to vary the gain as a function of counts was included in the program but not used because counts and lamp heat flux were relatively linear.

Open-loop control, also shown in Figure 10, was included as a backup to the primary system. The open-loop logic had to assume that count values necessary to produce required flux profiles could be determined and programmed before the actual test. Preprogrammed curves of counts versus time were included on the profile tape to drive the power controllers if the feedback loop failed and the open-loop control became necessary. To correct the predicted curves during test, an open-loop adjustment factor was included for each zone. The counts from the profile tape could be multiplied by the adjustment factor to obtain the required counts for the next interval. Predicted

counts and desired heat fluxes were recorded on the profile tape so that the control could be switched between the open or closed loop without disrupting the simulation timeline.

A third option, manual control, allowed direct entry of the lamp heat flux and was included for calibration and test-article conditioning. The computer converts the flux entry into counts using the closed-loop gain factor. This count level is maintained until a new flux is entered or another control option is called. Option selection is independent for each zone, allowing a mixture of options to be simultaneously in effect.

Simulator operation was monitored through alphanumeric cathode-ray tube (CRT) displays, event lights, strip chart recorders, and real-time printouts. CRT's provided real-time display of pertinent parameters for rapidly evaluating the simulation. Event lights announced all anomalies that were detected by the control program and indicated the control option in effect. Strip charts and printouts provided hard-copy records for near-real-time analysis. The test engineer monitored the simulation, selected the flux profile and the operating mode (closed, open, or manual), adjusted the closed-loop gain, and exercised other controls over the simulation program from a single control console.

The calibration radiometer (Fig. 11) was developed at MSFC to provide an economical sensor that could be used in quantity for mapping steady-state-absorbed, heat-flux distributions over surfaces of thermal vacuum test articles. The sensing element is a thin metallic disc, insulated in back, which in vacuum attains a thermal radiation equilibrium with its environment according to:

$$\left(\frac{Q}{A}\right)_{A_{B_S}} = \sigma \epsilon T^4 \quad .$$

The emittance, ϵ, of the sensing surface is known and the disc temperature, T, is measured by the thermocouple. If the sensing surface and test article are coated identically (and are thereafter subjected equally to any contaminating environment), the test article absorbed flux at the radiometer is monitored. If the surface absorptance to the incident energy spectrum is known, the incident flux may be determined by dividing absorbed flux by the known absorptance.

Radiometers used for mapping the absorbed flux distribution of the simulator employed a 0.032- by 1.75-in. diameter aluminum sensing element.

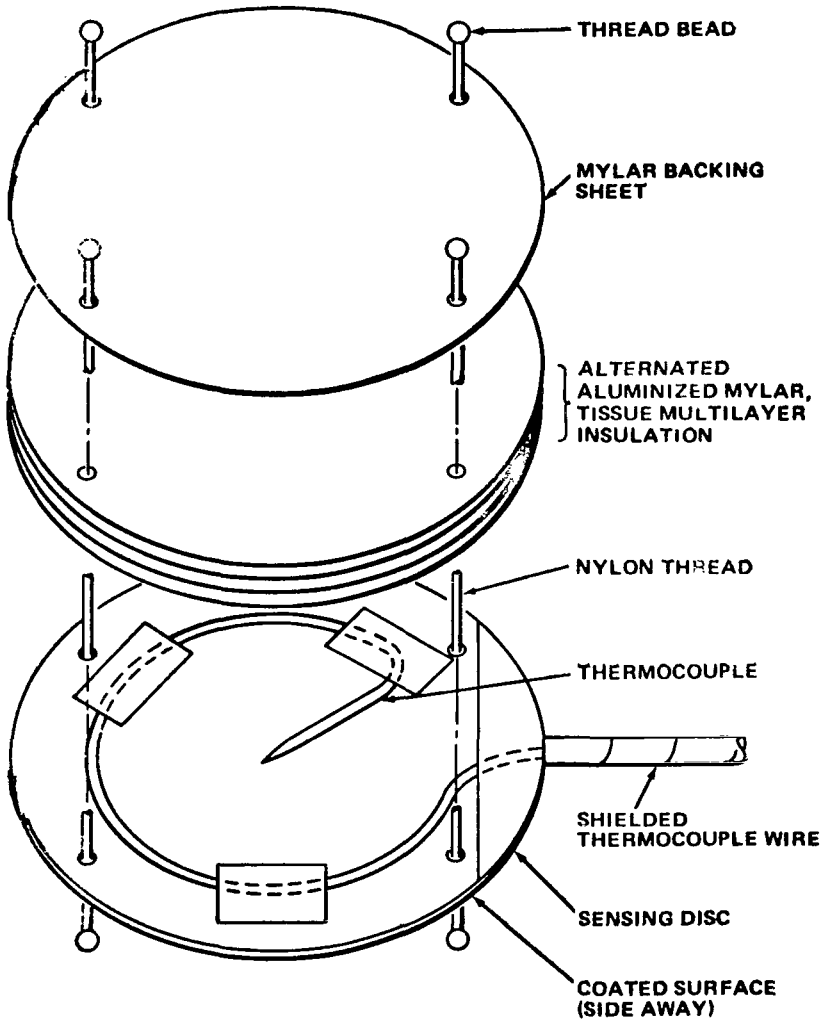

Figure 11. Calibration radiometer.

The coating has an emittance of 0.91 ± 0.01. Fine copper-constantan thermocouple leads were wrapped with aluminum foil for radiation shielding. Insulation was provided by layers of 0.25-mil aluminized mylar alternated with 6-mil sheets of tissue glass. A backing sheet, made of 14-mil mylar, provided rigidity. The assembly was fastened by nylon strands that were beaded on each end to maintain an insulation blanket thickness of 0.187 in. Hook and pile fasteners were used for attaching the backing sheet to the test article. Tests were performed on a number of radiometers to determine the magnitude of heat leakage through the insulation blanket and thermocouple leads which could result in errors in the measured flux. Under worst-case conditions, the combined uncertainty for the ATM TSU test conditions was found to be less than 1 Btu/hr-ft^2 which was within acceptable uncertainties for this application.

ON-SITE THERMAL SUPPORT

Pretest Activity

Before delivery of the ATM to Chamber A, the GSE was installed at the complex. This included power supplies, signal conditioners, experiment control console, etc. The ACE programs (software) were verified, and stimuli to the ATM were checked at the ATM cable interface using special test equipment. The ATM was installed in Chamber A, and electrical connections were made. The MDA end thermal cover and solar shield that were shipped separately were installed.

At this stage of pretest activity, thermal personnel were moved on site to monitor remaining activities before thermal vacuum testing. First, proper installation and operation of the calibration and OHS control flux sensors were completed and verified. The IR cage structure was then assembled around the test article. The IR lamp and the reflector assemblies were mounted to the structure and aligned. Several changes were required to complete the OHS installation because of such problems as physical interference between the test article and the OHS. Thermal personnel monitored the sensor installation and the OHS assembly and had final responsibility for all changes to assure that the OHS would provide the required environments.

Additional system checks were made by applying ATM power and by verification of the OHS operation under computer control. Photographs were taken of the ATM while being illuminated by the OHS to provide information on shadowing and uniformity. These ambient tests were conducted to verify that all systems were operational before vacuum testing. Personnel designated to monitor the ACE consoles received valuable training on equipment operation and procedures during this time. The pretest checkouts at ambient conditions provided excellent experience before the critical test sequences. As a part of pretest activity, a data process plan was prepared by MSC with MSFC concurrence which established the type, amount, and disposition of data generated during thermal vacuum testing. From delivery of the ATM TSU to MSC until completion of installation Chamber A, 45 days elapsed.

Test Monitoring

Continuous monitoring was necessary for all systems during the vacuum portion of the TSU test. The long test duration (323 hr) and around-the-clock testing resulted in three work shifts. The thermal personnel on each shift

were as follows:

1. One thermal supervisor.

2. Two OHS system engineers.

3. Two rack component analysts.

4. Two canister/experiment analysts.

The thermal supervisor has overall responsibility on thermal aspects of the test and assured that thermal test objectives were met. The OHS engineers were situated in the control room with the supervisor. Their task was to operate the OHS by issuing commands to the ACE computer and to monitor the system for proper operation. They also executed commands for the thermal uplink data display computer data printouts (THUDD). The rack and canister analysts monitored real-time and near-real-time data to assure that ATM systems were within limits, operating properly, and in the proper mode for each test. They also maintained selected plots of parameters for test control and determining equilibrium conditions. The rack and canister analysts were located in a data room which was removed from the control room. Real-time evaluation was by use of CRT's which included over 800 parameters displayed in digital format on 20 selectable pages. Five CRT monitors were used by the thermal group. THUDD printouts provided near-real-time data that were used to plot graphs and provide a permanent record of data during the test. The THUDD printouts contained 1343 parameters and were executed at intervals of 5 to 30 min, depending upon test activity.

Extensive pretest preparations were made for data evaluation and handling. Pretest predictions were made for most parameters for all steady state tests and for preoperational, activation, and cold soak tests. Selected measurements were chosen as test-control measurements, and computer-prepared graphs were made for all tests which had the ordinate and abscissa scaled and the predictions shown. These plots were used to chart the progress of each test with minimum labor. Overlays were prepared for each sheet of the THUDD printouts for quick retrieval of data. Also, several matrices were prepared to cross reference measurement numbers, stimuli, power dissipation, etc. This allowed data-room personnel to monitor the test in an orderly manner, troubleshoot, and to make real-time evaluation of ATM performance. During T/V tests, certain anomalies arose in TSU equipment and OHS performance which was detected by real-time data analysis. This information was reported to the thermal supervisor and test conductor for corrective action. In general,

real-time monitoring of vehicle performance was essential and gave confidence that each test run had met the test objectives within minimum test time. Confidence in the real-time data analysis was such that a post-test-data review was not held. The post-test evaluation did not reveal any significant test anomalies that were not discerned by the real-time analysis.

The greatest weakness in the real-time analysis was the poor resolution of the power dissipation of an individual component. This was due to ganging of several TMU's on one power buss and to long line lengths from the power measurement to the TMU.

Post-Test Activity

After the test was completed and Chamber A was repressurized, the vehicle was inspected with no significant discrepancies. The OHS was powered up to verify that all lamps were still operating. The TSU was then powered up at ambient conditions to check purge requirements. For this test, the large chamber door was open and the air temperature was about 65°F. The CBRM's exceeded their 86°F temperature limit at approximately 2 hr. No other component exceeded an allowable limit for the 6-hr duration of the test. This test concluded the test activity for the TSU. A final test report [5] was written covering all significant activities during the TSU test. The report covered TSU performance, personnel activity, and conclusions and recommendations.

A problem occurred during post-test-data reduction. Because of the large amounts of data being recorded, it was necessary (and desirable) to compress the data such that only a specified change in level would be recorded when converting the analog data to digital format. Data through run 10 were recorded on tape at a 4-bit change level (normal MSC recording tolerance) which required a 6.32°F change in some measurements before a new data point was recorded. This resolution was inadequate for thermal evaluation. Therefore, it was necessary to rerun the analog tapes to convert to a 2-bit tolerence. The conversion from analog-to-digital data is done on a real-time basis, resulting in considerable additional computer time and expense whenever reruns are required.

Photographic coverage of the TSU was made on a continuing basis throughout the test program. The coverage provided a historical record of events for future reference. These photographic data were extremely valuable to the thermal analyst during detailed data evaluation.

ORBITAL HEATING SIMULATOR PERFORMANCE

Orbital Heating Simulator Calibration

Calibration was performed at the test site under thermal vacuum conditions with the spacecraft and simulator installed. Requiring approximately 45 hr, calibration determined the performance parameters for the control program. These parameters included absorbed background heat flux (BHF), absorbed lamp heat flux (LHF), and absorbed total zone heat flux (ZHF) as a function of counts for each zone. In addition, primary and secondary heat flux sensor correlation factors (H and J, respectively) and the gain factors (D) were determined. Calibration also evaluated heat flux uniformity for post-test analysis. Flux mapping was accomplished by monitoring 389 calibration radiometers and 67 heat flux sensors.

In developing the simulator calibration procedure, ZHF was considered to consist of LHF and BHF. LHF is filament radiation which reaches the surface either directly or by reflection and is controlled through the applied power. BHF is stray radiation from surrounding structures, the spacecraft, the solar simulator, or the chamber. In the calibration procedure, all zones were powered simultaneously to a common prespecified count level and held for 4 hr to attain equilibrium of background radiation and calibration radiometers. Lamps were then alternately turned off, on, and off at 5-min intervals. The total sequence was performed at six different count levels.

Steady state readings at each count level were used to obtain heat flux uniformity maps, and were also area integrated to define ZHF as a function of C.

The H and J factors are used by the control program which relate the heat flux measured by the sensor to the true average heat flux over the corresponding zone. Intermediate primary and secondary sensor correlation factors were calculated at each count level according to:

$$H, J = \frac{ZHF}{\text{Primary and secondary sensor readings}} \quad .$$

As shown in Figure 12, these intermediate values were plotted against ZHF and final values were taken as the average of the intermediate values within the range of the mission flux profile.

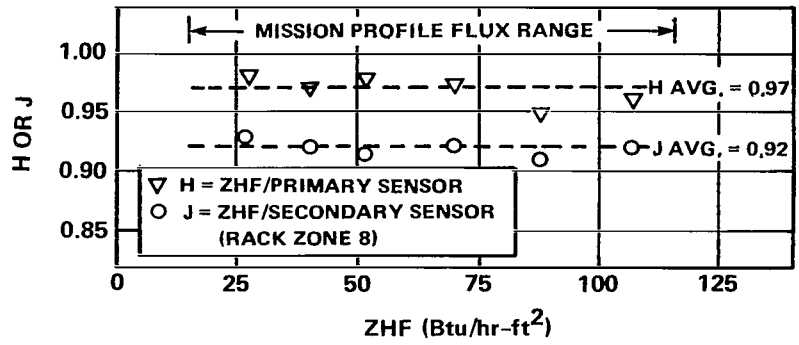

Figure 12. Correlation factors.

The absorbed LHF at each count level was determined from the on-off sequence data. One-minute sensor readings were corrected using H and J and plotted against time as shown in Figure 13. LHF contribution to the ZHF is the absolute difference between the initial and a later value of ZHF following the turning-on or turning-off of the lamp bank. The time dependent differences for the three 5-minute intervals are overlayed as shown on Figure 13 to obtain an average. Curves, typified by Figure 13, showed the major heat flux response occurred within 3 min of the step change in lamp power. Accordingly, 3-min values were treated as LHF and plotted against counts. D, another parameter of the control program, represents short-term heat flux response to a change in C and was evaluated as the sloped LHF versus the C curve (D = $\Delta C/\Delta$ LHF). BHF was calculated at each count level as the difference between ZHF and LHF (BHF = ZHF - LHF). A typical correlation for the rack is shown in Figure 14.

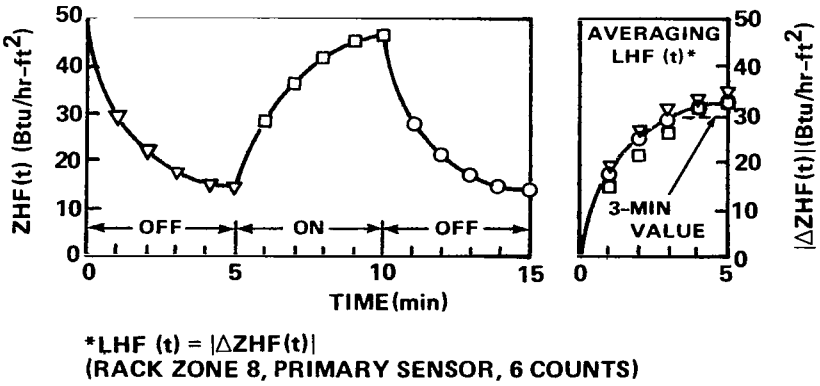

Figure 13. Average lamp flux response.

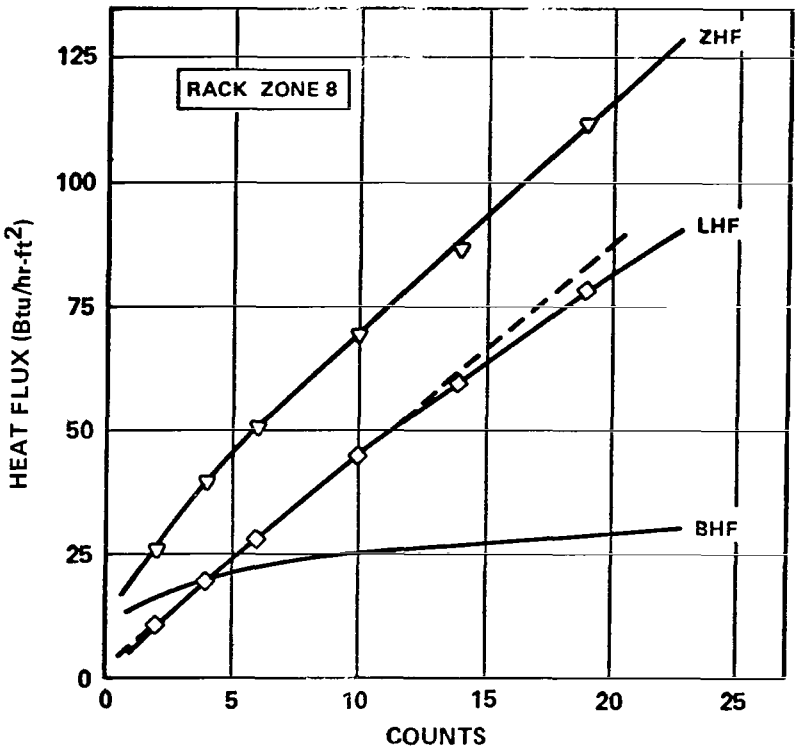

Figure 14. Heat flux correlations.

The orbital heating simulator performed satisfactorily during the calibration tests, and required performance parameters were evaluated from the resultant data. Several design deficiencies concerned with poor power resolution and high background levels were discovered during the calibration, but did not significantly degrade the subsequent simulations.

Flux distributions mapped during the calibration were very similar to those predicted by the mockup tests used in the design phase. Examples of typical normalized flux distributions for the radiator and rack are shown in Figure 15 and 16, respectively. The exceptionally close agreement depicted in Figure 15 between the mockup vacuum run and the calibration test illustrates the ability to obtain repeatability between two separate runs. Analysis of the ambient and calibration (vacuum) flux distributions obtained for the rack (Fig. 16) shows the vacuum distribution as being more uniform, especially along the zone perimeter. This indicates that background (IR) radiation, which was not included in the ambient map, enhanced the overall uniformity. In general, the good agreement obtained between calibration and mockup testing accentuated the value of the simulator's experimental design phase.

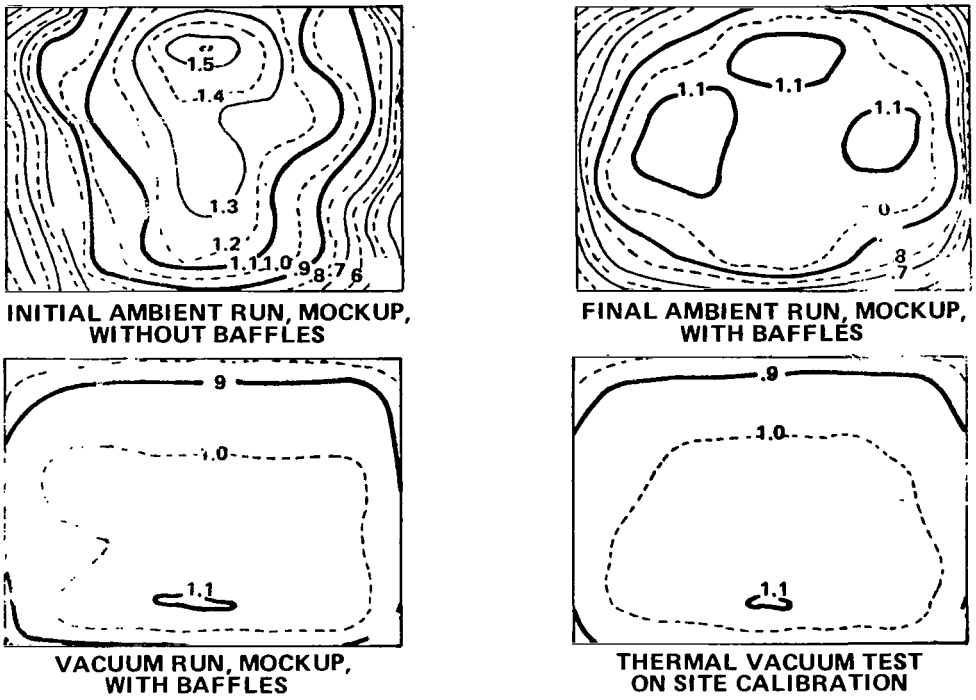

Figure 15. Uniformity evolution, radiator normalized flux distributions.

An analysis of the on-off sequence data used to determine the LHF curves (Fig. 13) indicated that the LHF and BHF are not easily separable. If BHF were constant, the overlay would stabilize within 1 to 2 min. Since the flux was still changing after 5 min, BHF had transient components which responded less rapidly than the lamp filaments. The relatively slow response of the lamps, 80 to 90 percent in 3 min, is probably caused by a lag in the rise and fall of the quartz envelope temperature since the quartz has an effective emissivity greater than 0.85 for a temperature less than 1200°F. Although the reflector body would also experience temperature excursions significantly slower than the filaments, the low emissivity of the gold surface (typically less than 0.1) would dampen out this contribution. At the low power levels used by the simulator, the filament radiation shifts into the infrared region where the quartz transmissivity is near 70 percent. Thus, approximately 30 percent of the filament output is absorbed by the quartz and reradiated at a longer wavelength or conducted through the mounts. Since quartz has a low thermal conductivity, the latter is probably negligible. The long-term transient background, indicated by the continued rate of change after 5 min, was

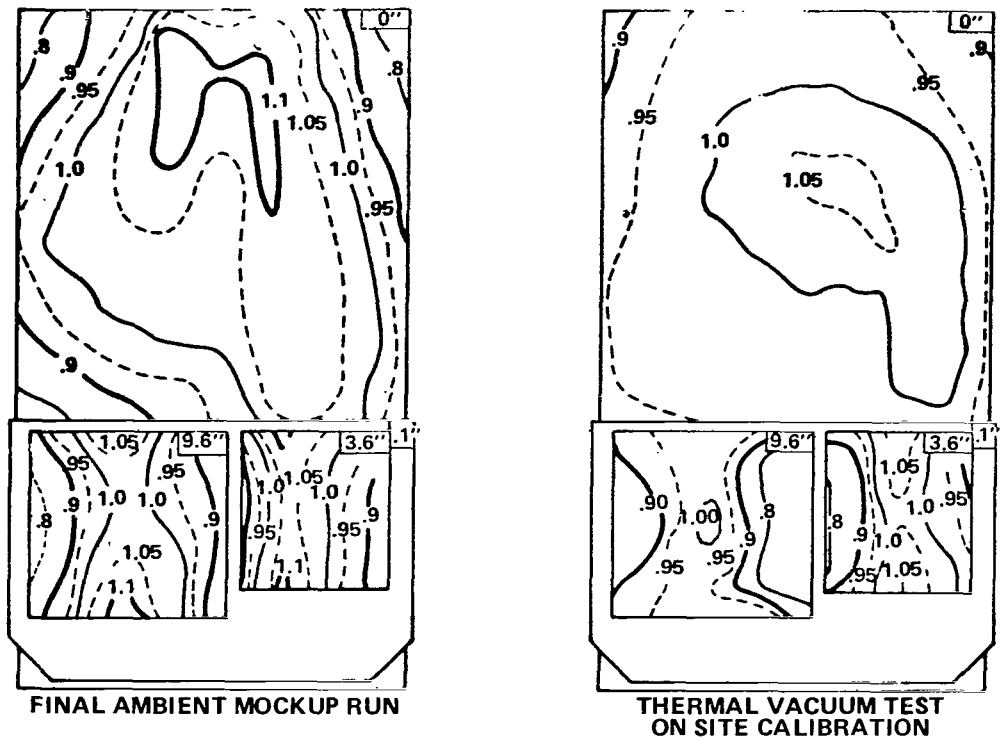

Figure 16. Uniformity evolution, rack normalized flux distributions.

because of the heating and cooling of surrounding structures, including the solar panel support structure, baffles, and the IR cage. In the lower radiator region, it was necessary to place the lamps close to the surrounding solar panel support structure to achieve the desired uniformity on the radiator. As a result, the support structure received excessive heating, not only producing the long-term transient backgrounds, but also causing an undesirably high level of background. The alzak baffles, used extensively in the radiator zones, aggravated the problem because of their high absorbtivity and emissivity in the long wavelength region (typically 0.7). As shown in Figure 17, the background radiation was approximately 40 percent of the ZHF at nominal heat flux levels. This high level of background in the radiator zones, coupled with the slow response time, had two implications. First, the closed-loop concept for the control program was essentially mandatory since an open-loop control could not cope with the sizable and unpredictable background. Second, descending flux transients and minimum flux levels might be difficult to simulate. Previous mockup tests, however, had shown the lamp and baffle configuration necessary for meeting uniformity and minimum overlap requirements. Since there were

deemed more important for simulator control and post-test environment analysis, the compromise of high background was accepted.

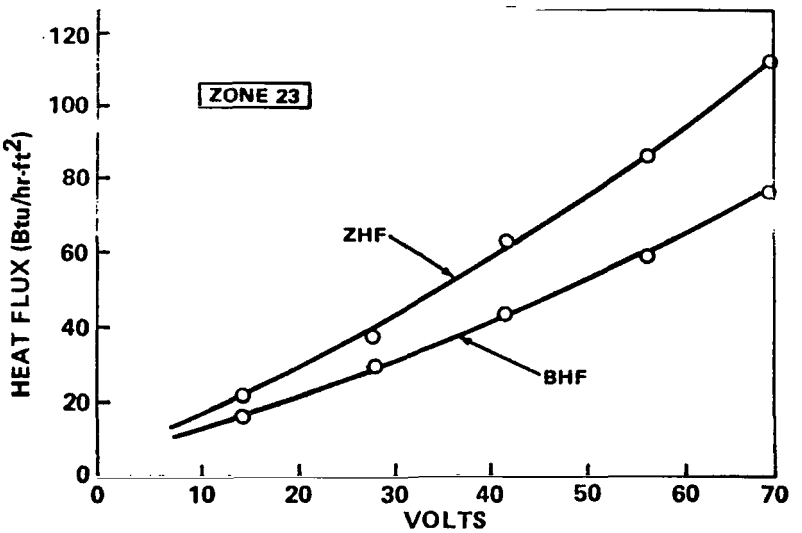

Figure 17. Heat flux correlation radiator mockup vacuum test.

During the calibration test, the simulator proved to be more efficient at lower power levels than anticipated, resulting in a loss of power resolution. Based on a 63-count power division, an average power resolution of 3.2 Btu/hr-count would be obtainable for the maximum design flux level of 200 Btu/hr, assuming a linear relationship between ZHF and C. However, a typical ZHF curve (Fig. 14) shows a resolution of about 6 Btu/hr-count at lower flux levels. Initially, it was surmized that the lamp array was over-designed more than anticipated. Subsequent data obtained in the thermal vacuum test showed that the maximum attainable heat flux on a typical rack zone was only about 235 Btu/hr. As indicated in Figure 18, the poor resolution at the lower count levels was caused by a nonlinear heat flux to count response rather than an over design. The reason for the response curve is not clearly understood. A decrease in the absorptivity of S-13G at higher levels (because of the spectral shift of the filament radiation) would produce the same trend as shown in Figure 18, but at a lesser magnitude. Apparently, this type of response is a characteristic of the particular lamp-controller combination.

The open- and closed-loop control options were also tested during calibration. Figure 19 shows the input flux profile and typical tracking results. The open loop run assumed a constant BHF that corresponded to the average

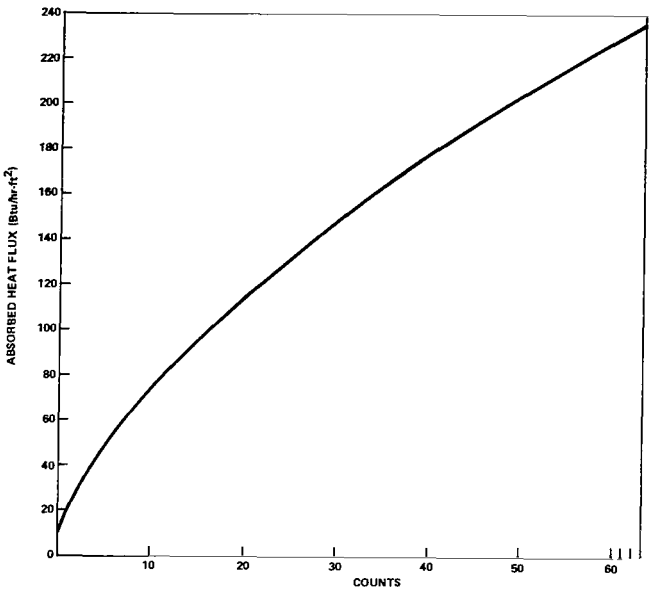

Figure 18. Total zone heat flux control characteristic.

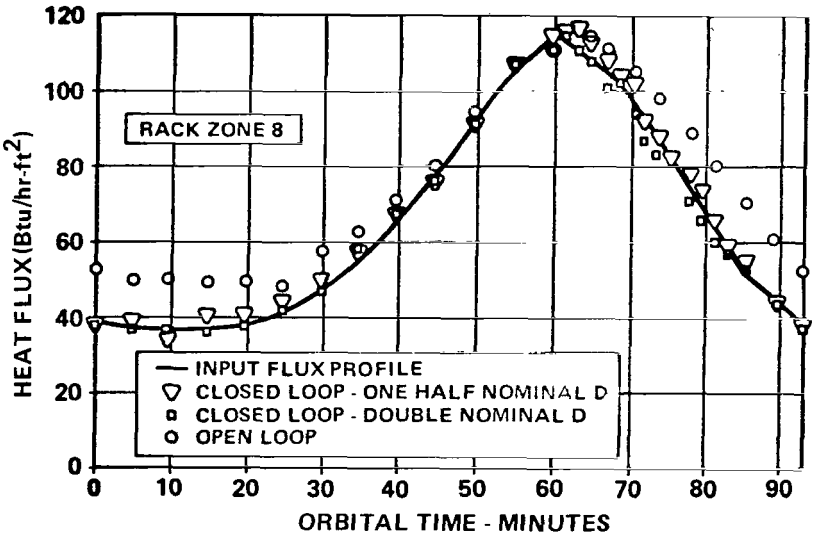

Figure 19. Calibration profiles.

ZHF of the input profile. As expected, the open-loop profile was distorted and lagged the input profile. However, the closed-loop control performed satisfactorily for variations in D of -50 to 100 percent from the nominal calculated value.

Orbital Heating Simulator Test Results

During all ATM TSU tests, the closed-loop control was used exclusively for flux regulation, thus avoiding anticipated difficulties of the open-loop option. Fluxes in steady state tests were simulated, on the average, within ±1 Btu/hr-ft^2. The poor power resolution of 6 Btu/hr-count was compensated for by the closed-loop control system which alternately selected successive count levels to obtain the desired average flux level. Typical tracking results for transient runs are presented in Figure 20. The closeness of the simulation demonstrates the ability of closed-loop control to correct for large background transients. Certain radiator fluxes failed to reach minimum levels during cold-case transient runs when the background exceeded these minimums. The manual control option was used for the test article conditioning before certain tests runs and also proved invaluable in maintaining environments on several occasions when the ACE complex suffered short malfunction periods. Three primary sensors gave anomalous readings during the test and control was switched to the secondary sensors.

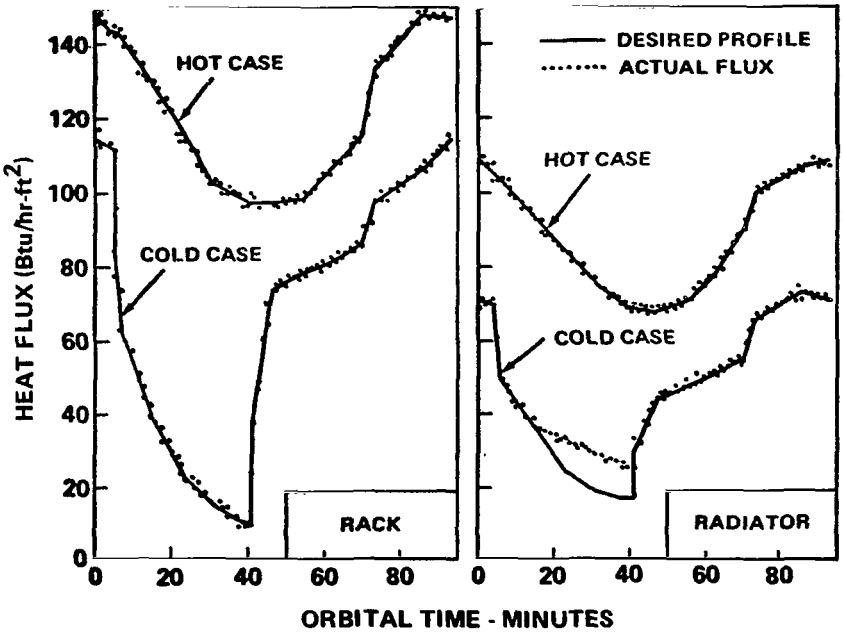

Figure 20. Profile tracking results.

The simulator performance has proven that digital closed-loop computer control of orbital heating simulators using heat flux sensor feedback is an effective tool in tracking both steady state and transient flux profiles. The effectiveness is accentuated when a variable background degrades flux predictability for open-loop programming.

VEHICLE TEST PERFORMANCE

Test conditions and observed test performance are discussed in this section. A more detailed discussion of test data, test anomalies, and required design changes is discussed later.

Evaluation of the vehicle performance showed that none of the rack components exceeded the upper temperature limits. Six components exceeded the lower limits, contrary to pretest predictions. The NRL-A, NRL-B, and HCO-A telescopes were within limits for all tests. The H-α telescopes were cold biased because of an apparent degraded gold coating and the AS&E telescope ran hot because of a malfunctioning thermal control system. The GSFC telescope was within allowable limits when solar heating was present on the solar shield. For the HAO telescope, the TV cameras and film cameras experienced some out-of-limit temperatures. The canister TCS performed adequately, thereby maintaining the cold-plate inlet temperature within the desired range of 50 $\pm$1°F.

The thermal vacuum tests were identified as Runs 1 through 14 as noted earlier. Run 1 was used to calibrate the OHS and was not used to evaluate vehicle performance. The following paragraphs briefly describe the TSU performance for Runs 2 through 14. The tests are described in the sequential order in which they were conducted.

Run 2 - Cold Soak

This test did not simulate any Skylab mission but was devised for model correlation. All TSU and OHS power was off. The test began with the TSU at approximately 70°F. The upper radiator OHS was activated at 6.75 hr to prevent freezing of M/W. The canister interior response was slow because of the insulation, and at test termination the spar was still cooling at approximately 0.25°F/hr. The test was terminated at 12 hr since many of the rack components were approaching -100°F. External rack components and the radiator did not cool as rapidly as predicted because of background radiation.

Run 3 - Steady State Extreme Cold Environment

For this run, no power was applied to the rack components and canister TCS; however, telescope's TCS and vidicons, and canister rate gyros were activated. Satisfactory thermal equilibrium was achieved in the 53-hr test duration. Over 90 rack-mounted components stabilized well below their lower allowable storage temperature limits. No thermal design problems were indicated since the condition tested is not a planned mode of operation; however, it shows that a power-off storage mode is not feasible for the rack components. The H-α vidicon exceeded its temperature limit during this test. The fine sun sensor control electronics, located on the MDA end of the canister, exceeded lower limits during the test; however, the lower limit of this component has been reduced to alleviate the storage temperature problem. There will not be a freezing problem with the M/W during orbital storage.

Run 4 - Steady State Extreme Cold Environment

This run simulated a possible cold orbital condition with all rack components powered up, the canister fluid TCS on, the experiment TCS heaters on, the canister equipment duty cycled on standby mode, and the solar simulator on. Satisfactory thermal equilibrium was achieved in the 35-hr test duration.

The components requiring additional thermal conditioning as a result of low temperatures during this test were the acquisition sun sensor and electronics located on the sun pedestal, a remote analog submultiplexer, and tape recorders. The Hα-1 telescope vidicon again exceeded its upper temperature limit as in Run 3. Both Hα-1 and Hα-2 were below temperature limits because of the degraded coating. The HCO-A and GSFC experiments also ran cold.

This was the first run with the canister TCS active. Upon activiation, the system was unstable with the canister inlet temperature oscillating between 45.5° and 52.5°F. The dither box (electric oscillator to continuously stimulate the modulating flow control valve) was activated, but the temperature oscillations continued. The primary TCS (valve, heaters, and pump) was deactivated and the secondary TCS was activated. The canister inlet temperature was still unstable. The dither box was cycled several times. However, the instability remained at approximately 2.5°F peak-to-peak at 3 cycles/min. The dither box gain and frequency were varied through several settings. At a setting of 0.5 cps and 0.8 V (peak-to-peak), the oscillation was reduced to approximately 1.5°F which was considered acceptable for TSU testing. The TCS radiator was approximately 10°F warmer than expected; however, all cold-plate temperatures were within allowable limits.

Run 5 - Transient Extreme Cold Environment

The transient flux for Run 5 had an average value that was established during Run 4. The rack TMU's oscillated about the temperatures of the previous run. The excursions were as much as ±20°F for some of the exterior TMU's and less than 3°F for those in insulated bays. As previously noted, some TMU out of limit conditions persisted for the rack and canister during this test. Test duration was 12 hr.

Run 6 - Steady State Nominal Hot Environment

The environment for this test simulated a β angle of 75.5 deg. All of the rack TMU's operated within allowable temperature limits, assuring proper control for nominal heat environments. The fluid TCS maintained the desired control of the cold plates but the experiments warmed somewhat because of a change to the active operation mode. None of the Hα-1 temperatures were low, but the vidicon exceeded the upper limits. The Hα-2 and the GSFC experiments had some measurements that were still too cold. Also, the AS&E mirror housing and HAO film camera exceeded upper temperature limits. The run duration was 44 hr.

Run 7 - Transient Nominal Hot Environment

This run was a transient test under hot environmental conditions with all components active. The IR cage was cycled to simulate orbital transient heating, but the solar simulator was operated at a steady power level since the hot condition is a nonshadow orbit (high β angle). Rack component temperatures oscillated about the temperature levels already established by the preceding steady state tests, and all components remained within operating temperature limits. A test duration of 10.5 hr (7 orbits) was required to achieve all test objectives.

The canister TCS was active, and the experiment TMU's were in an operational mode, with the experiment thermostatic heater temperature control systems activated. All canister systems functioned normally within the design limits, with the exception of the components mentioned in Run 6.

Run 14 - Liquid TCS Failure

The environment for this test was a transient extreme hot condition which imposed a ±75.5 β angle, depending on which established the higher heat flux on each OHS zone. The test was begun with the temperatures established in Run 7 by turning off the fluid TCS. The AS&E telescope was out of limits 2 hr after start of the test, the GSFC at 5 hr, and HAO optics at 6.5 hr. The HCO-A, NRL-A, NRL-B, Hα-1, and Hα-2 generally were within limits at 6.5 hr at which time the test was terminated.

Run 8 - Steady State Extreme Hot Environment

This run was a steady state extreme hot environment test with rack and canister components off. The extreme hot environment is a composite condition composed of the hottest environments for each of the individual rack and radiator zones. Since these conditions will occur at different times in the actual mission for each zone, a simultaneous application of these environments composes a conservative test condition. However, thermal coupling between the adjacent rack zone is, in reality, insignificant and a considerable reduction of test time was realized. Thermal equilibrium was achieved satisfactorily in the 42-hr test duration. The tape recorders and the CBRM's fell below allowable storage temperatures. All experiment temperatures except the Hα-1 and Hα-2 vidicons were within limits. This could be partly attributed to the zoom drive power being inadverternly left on during the test.

Run 9 - Steady State Extreme Hot Environment

With all component power on for this test, the rack TMU's again warmed considerably and all rack components operated within limits. This was the only test during which the massive CMG's stabilized. Experiment temperatures were exceeded for the AS&E mirror assembly and the camera vidicons for the HAO, Hα-1, and Hα-2. During this test, the AS&E TCS failed to operate properly. Some difficulty was experienced with instability of the fluid TCS, but temperature control of the fluid within its allowable limits was maintained. The duration of the test was 30 hr.

Run 10 - Transient Extreme Hot Environment

The rack TMU's oscillated about the values established in the previous run with all units within limits. Thermal problems encountered with the experiments were similar to those in Run 9. The fluid TCS instability reappeared and required manipulation of the electronic controls to achieve a stable condition. Test objectives were satisfied within 8 hr.

Run 13 - Z Local Vertical

This test was designed to simulate the heat fluxes occurring during earth resources and docking maneuvers. Approximately 240 Btu/hr-ft^2 was imposed on each OHS zone for 30 min of two consecutive orbits and for 50 min of the third. At the 50-min point of the third orbit, 4 hr in the run, the test was terminated because the radiator temperature had reached 100°F. At this time, the hottest of the CBRM cells had reached 111.5°F.

Runs 11 and 12 - Pre-Operation and Activation

These two runs were transient cold environment tests conducted to simulate orbital insertion and activation of the ATM. Rack TMU's were activated at 2 hr and the canister at 7.8 hr. All rack TMU's were within limits during the tests except the active tape recorder. The test verified that rack components must be activated within 2 hr of launch. The HAO, HCO-A, GSFC, NRL-A, and NRL-B experiments were within limits throughout the tests. The Hα telescopes were within limits except for the TV camera. The AS&E experiment did not reach operational temperatures until 4 hr after activation. During this test, the canister thermal areas of concern were freezing of the TCS radiation coolant and excessively low experiment temperatures. Also, a prime objective was to determine the maximum time required to stabilize the experiment temperatures before solar observation. For the conditions tested, it appears that is will require approximately 20 hr from the time the experiments are on standby until they become thermally stable.

The canister TCS operated with the usual small amplitude oscillations that were observed in all the other runs. The data indicate these areas of concern will not be a problem.

Ambient Power-On Test

The purpose of this test was to evaluate purge requirements for the rack components during checkout. The chamber temperature was about 65°F and the large chamber door was open during the test. Results of the test indicate that the only rack components which will overheat within 6 hr are the CBRM's, which run as much as 10°F above their upper temperature limit. The 86°F limit was exceeded at approximately 2 hr.

In summary, of the 140 components located on the rack, 6 required minor redesign to maintain acceptable temperatures under cold conditions. No rack hot problems were encountered during the test which directly reflects the design philosophy of cold biasing the thermal design. For the canister, five of the eight telescopes were out of allowable temperature limits at some time during the TSU test. However, several test anomalies were identified which contributed to these discrepancies, particularly for the film and television cameras. In addition, the out-of-limit temperature excursions were, in general, small (on the order of 1° to 3°F). These excursions would not cause a catastrophic failure, but could degrade the scientific data.

DATA CORRELATION

Analytical and test data were correlated to verify the modeling techniques used and to update the mathematical models to make them representative of the physical system. Correlation procedures and results are briefly discussed in the following paragraphs. More detailed analysis can be found in References 6, 7, 8, 9, and 10. All test data can be found in References 11 and 12.

The initial effort for the post-test model correlation was to update the simulation of the chamber environment. One of the pretest assumptions was that all fluxes incident on the test article surface were emitted from the IR lamps; i. e., the background flux was zero. This assumption was known to be in error before the test. However, rather than make an estimate of the background level in the chamber, it was considered better for test monitoring purposes to know that all predicted temperatures were cold biased. To properly simulate the chamber environment, it was necessary in the post-test analysis to divide the measured flux into lamp and background fluxes. The background flux was determined from the IR lamp calibration data and was utilized to calculate equivalent environment tenperatures for each IR zone. A hemispherical enclosure, at the equivalent temperature, surrounding each IR zone was used in the mathematical model to simulate the background flux. The difference between total measured and background flux for each zone was considered as lamp flux.

Initial verification of the test environment modeling techniques was achieved with power-off, steady-state test data. These tests were chosen for environmental correlation because they eliminate two possible sources of errors: capacitance and component power dissipation rates. Following the component power-off data correlation, steady-state test data were correlated with the component powers activated.

The next step in the data correlation was to adjust the model capacitance by using data from the cold soak test which eliminated power and flux simulation uncertainties. The cold soak test consisted of preconditioning the test article to approximately 70°F. After the test article had reached a uniform 70°F temperature, the IR cage and all test article power was turned off and the test article allowed to cool. Caution was exercised to ensure that background flux was properly simulated since the IR cage was used to precondition the test article before beginning cold soak. If the background flux is not accurately simulated in cold soak correlations, the difference in slope between the test and analytical temperatures may be interpreted as a capacitance mismatch. Upon completion of the cold soak test correlations, correlations for the transient orbital tests were made.

Rack Correlation

Post-test analysis for the rack was performed by correlating the rack model with test results from steady state Runs 3, 4, 6, 8, and 9 and transient Run 11. Correlations of rack temperature are summarized in Figures 21, 22, and 23. These figures present representative pretest predictions from Reference 11 and post-test analysis from Reference 6. If the model correlated perfectly, all data points would be on a 45-degree line through the origin. A comparison of Figures 21 and 22 illustrates the improved model correlation as a result of the post-test analysis. Figure 23 demonstrates the good correlation of the math model with the test data over a wide temperature range. The distribution of model/test data deviations for each of the steady state runs as a result of post-test correlation is shown in Figures 24 through 28. These figures show that 14 to 26 percent of all correlations are within ±1°F, 55 to 80 percent are within ±5°F, and 86 to 98 percent are within ±10°F.

A zone-by-zone description of the steady state and transient model correlations follows.

Zones 1 Through 8 (Rack MDA End). The MDA end of the rack consists of 5 equipment shelves containing a total of 12 components. During Test 4, three components (main electronics assembly, star tracker optic-mechanical assembly, and the remote analog submultiplexer) were operating near or below

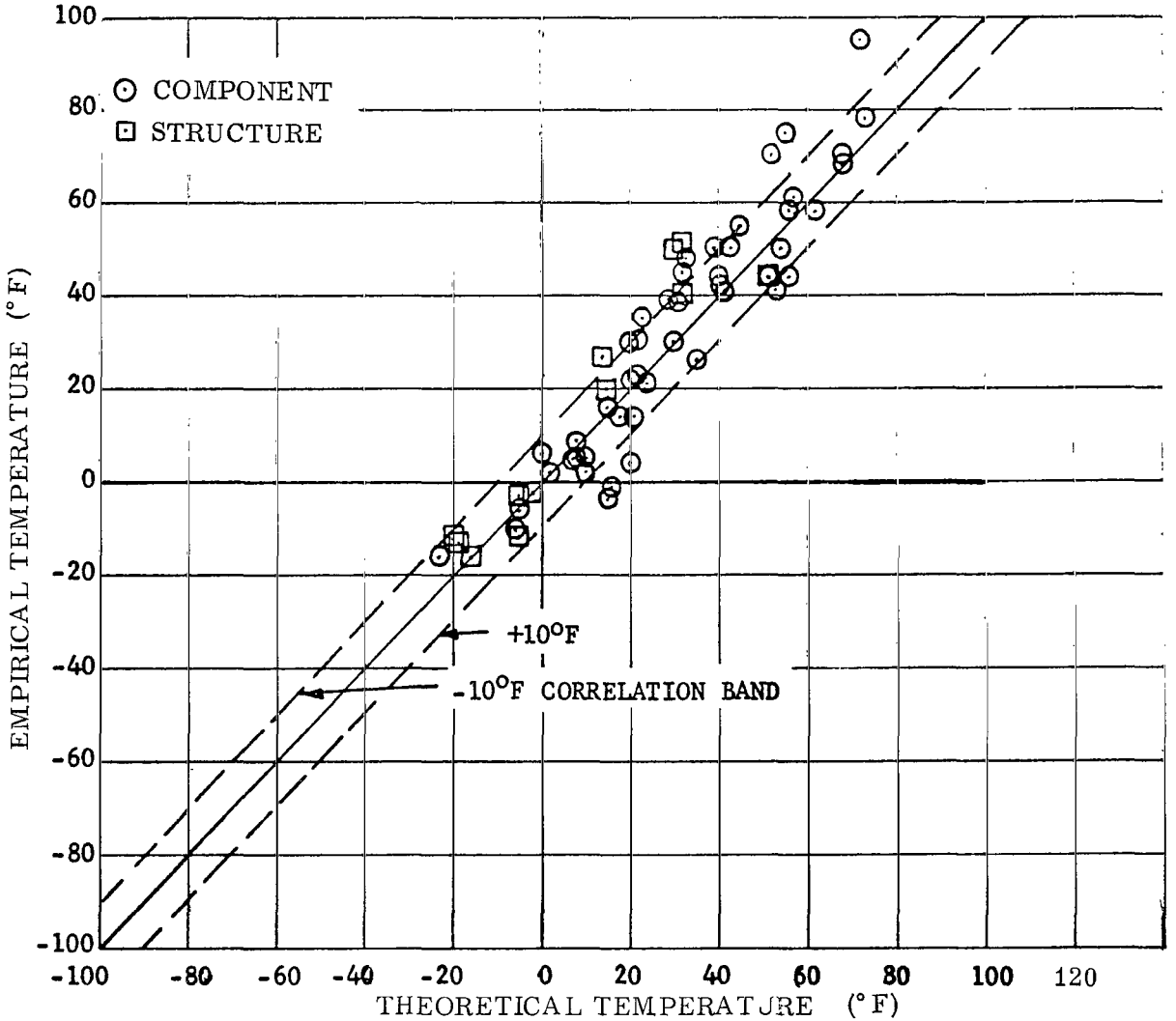

Figure 21. Rack component and structure comparisons of empirical temperatures and pretest theoretical temperatures for TSU Runs 4 and 9.

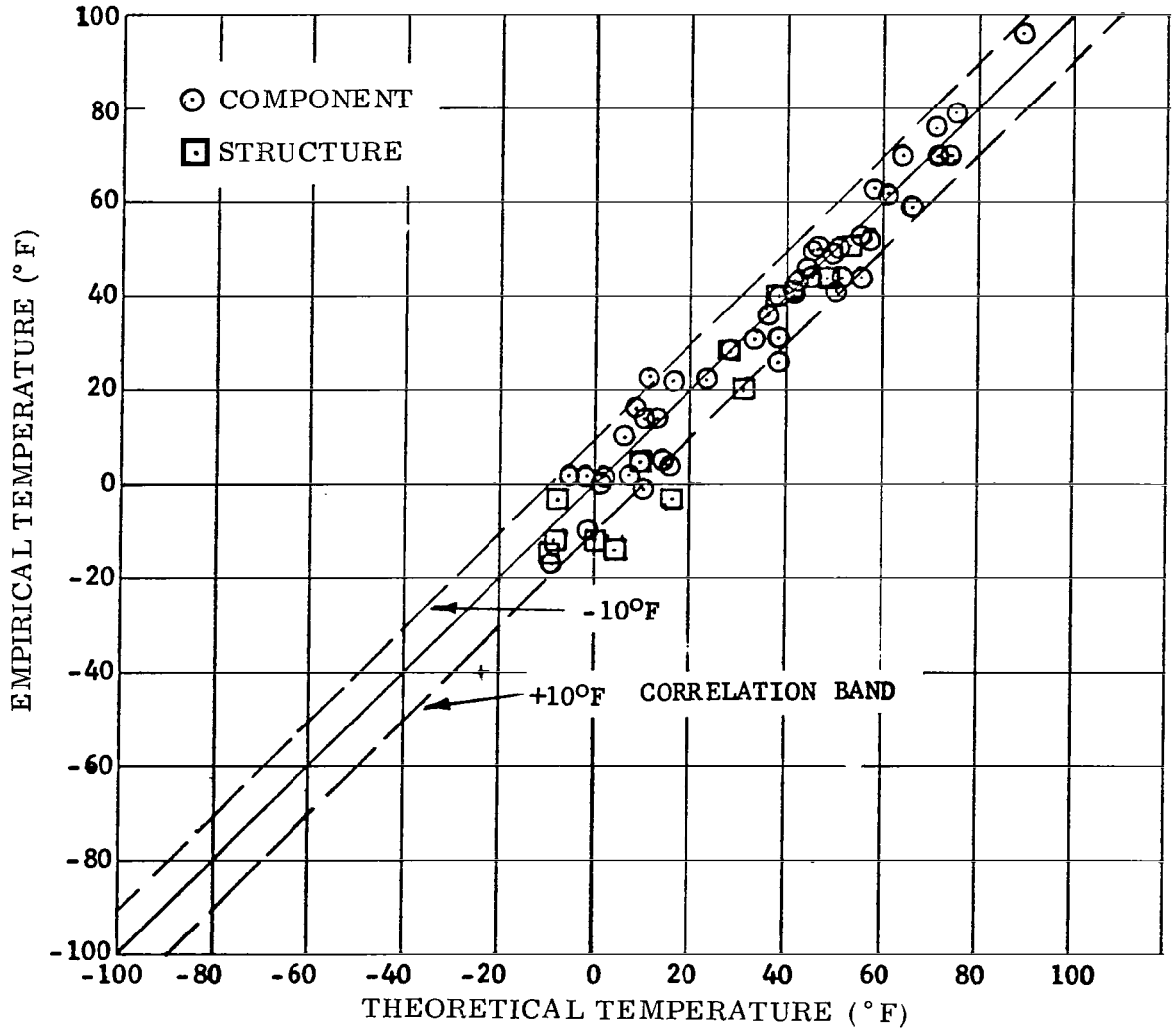

Figure 22. Rack component and structure comparisons of empirical temperatures and post-test theoretical temperatures for TSU Runs 4 and 9.

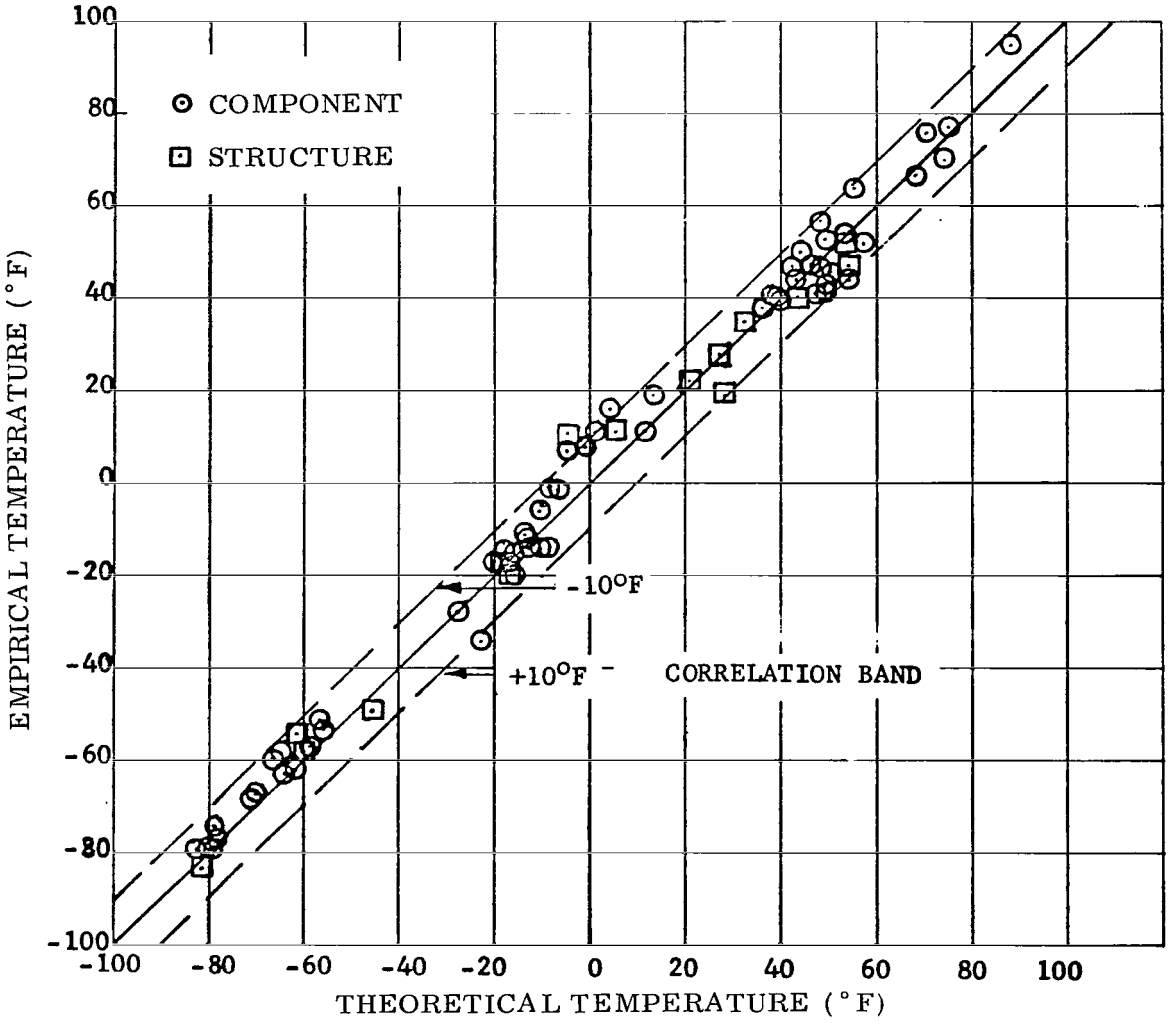

Figure 23. Rack component and structure comparisons of empirical temperatures and post-test theoretical temperatures for TSU Runs 3, 6, and 9.

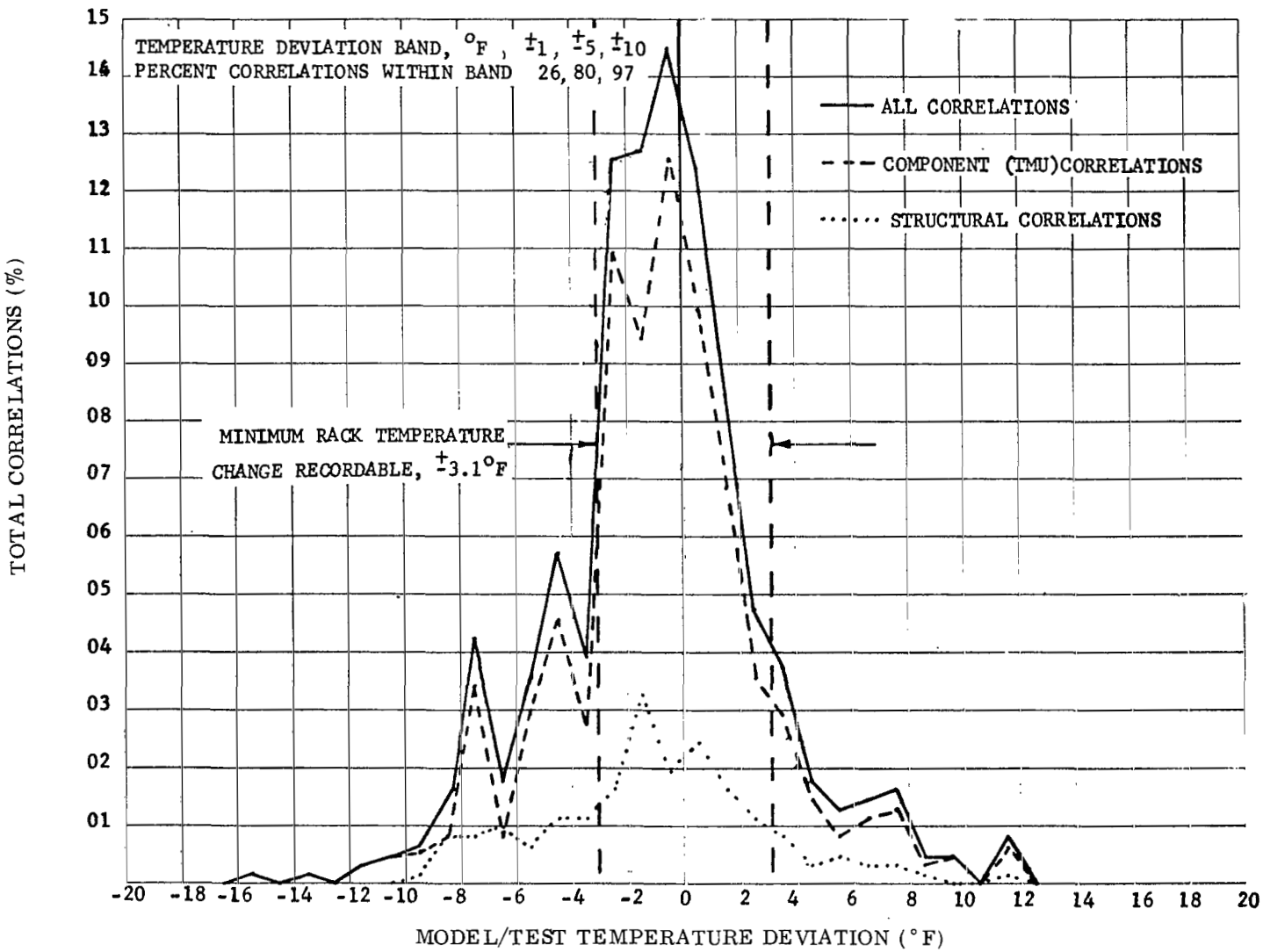

Figure 24. Run 3 distribution of post-test rack model correlations with test data.

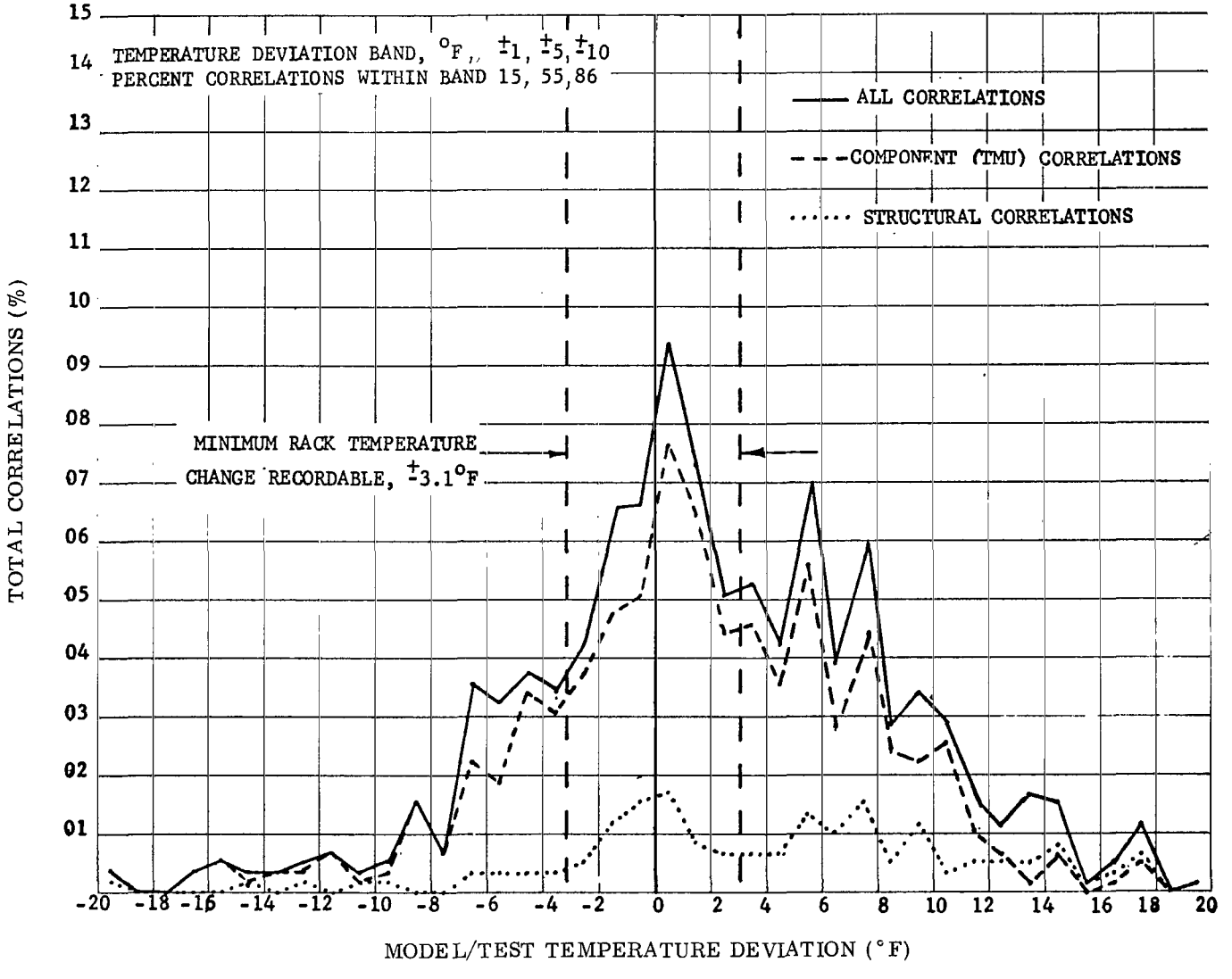

Figure 25. Run 4 distribution of post-test rack model correlations with test data.

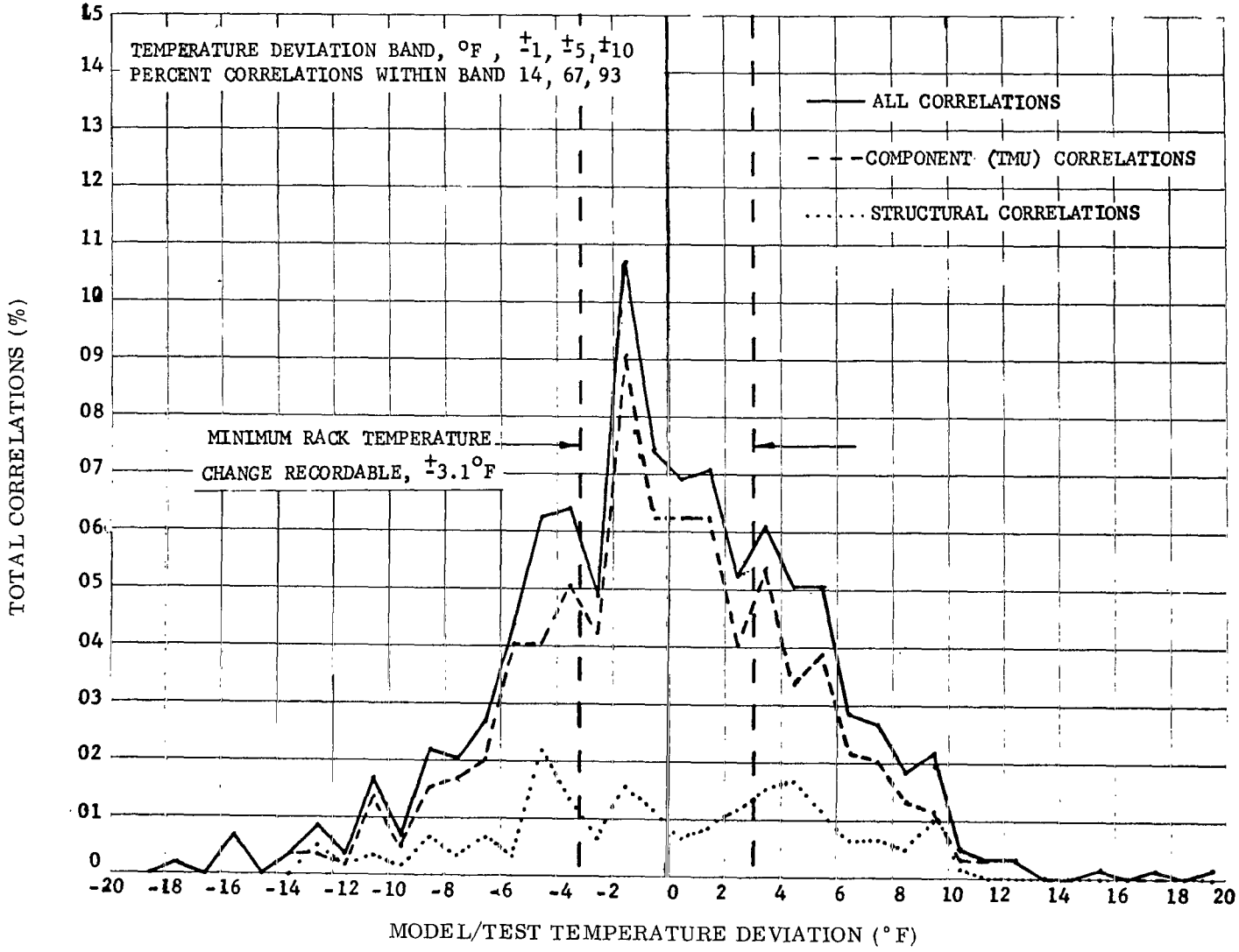

Figure 26. Run 6 distribution of post-test rack model correlations with test data.

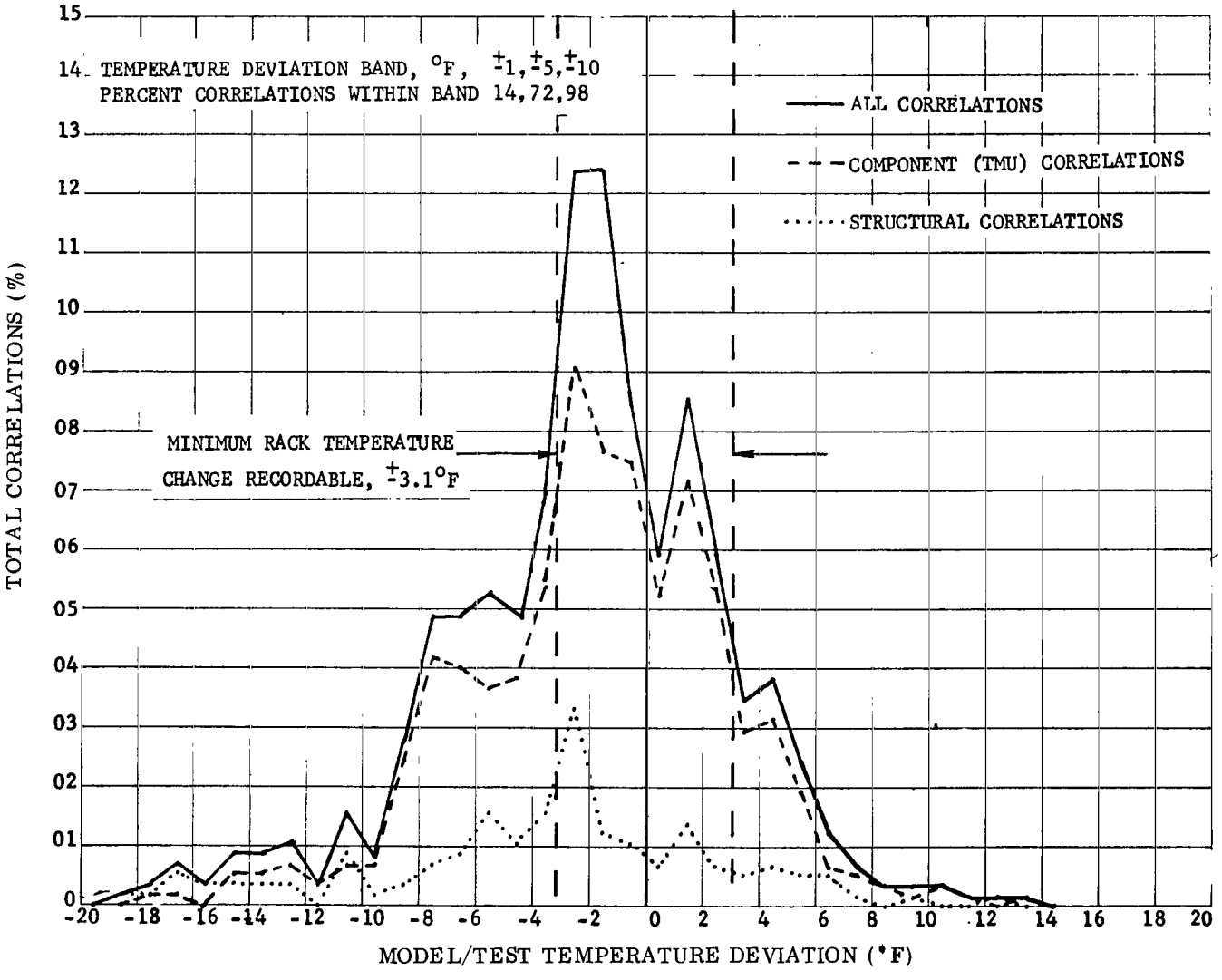

Figure 27. Run 8 distribution of post-test rack model correlations with test data.

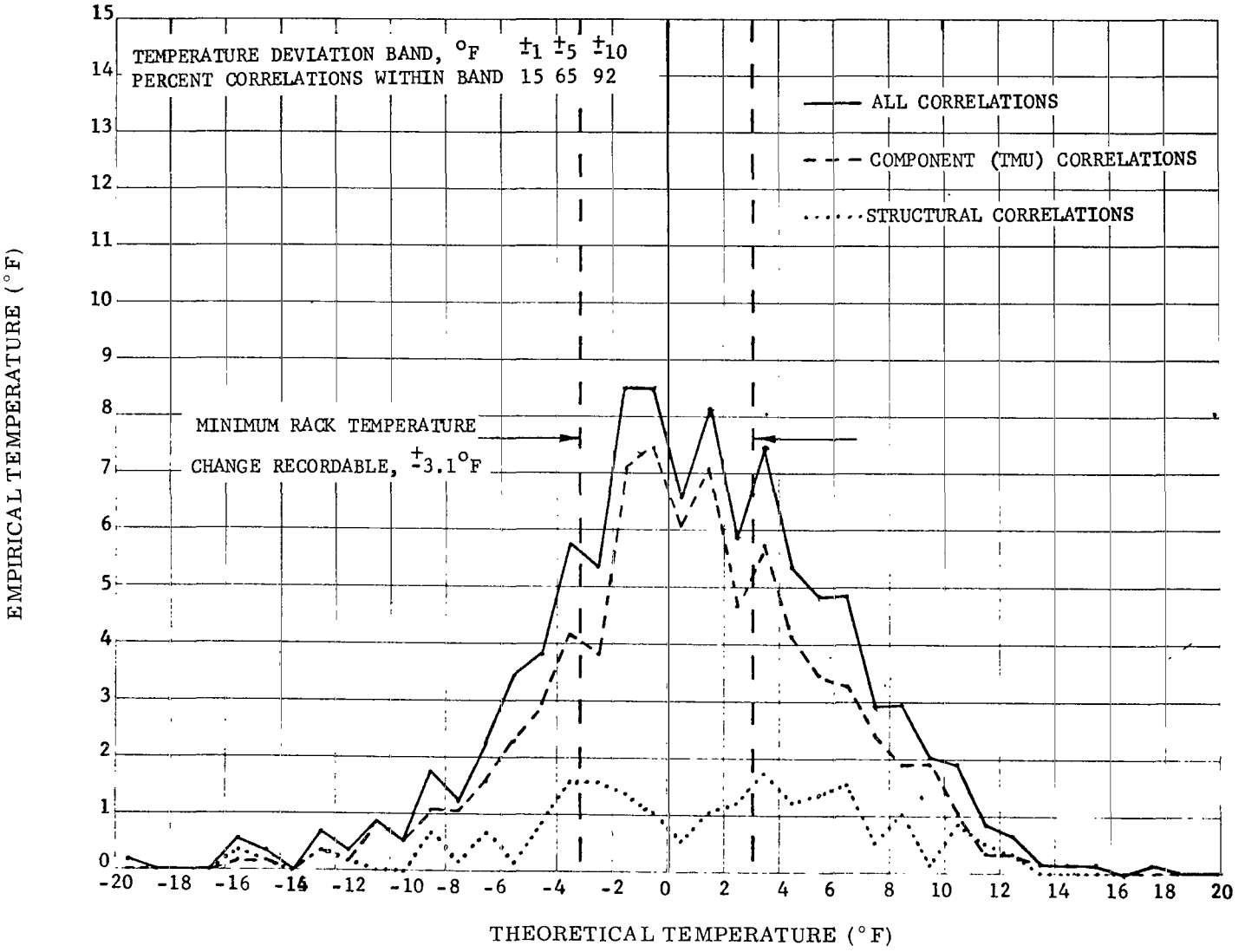

Figure 28. Run 9 distribution of post-test rack model correlations with test data.

their minimum temperature. Heaters are being added to all three components to correct this problem. In general, the temperature agreement between the test and analytical data was within 10°F.

Zones 9, 13, and 15 (CMG's). The large mass and the use of multilayer insulation resulted in the CMG's being in a nonequilibrium condition for all tests except Test 9. During Test 4, the CMG's operated below or close to their minimum operational temperature limit. This did not constitute a thermal problem since the TSU CMG's did not have internal heaters which are in the flight CMG's. If the heaters had been available on the TSU CMG's, the CMG's would not have exceeded their lower temperature limit. The analytical models predicted temperatures which agreed within 10°F of the test data.

Zones 17, 21, and 23 (CBRM's). Each zone contains six CBRM TMU's. Each CBRM is equipped with a thermostatically, proportional controlled heater. The heater control band is between 32° and 41°F. All CBRM's remained within their allowable temperature range except for module Number 2 in Zone 17 which experienced a heater failure. Since the heater failed while off, the module operated below its lower temperature limit during the cold environment tests. Internal power dissipation rates maintain the CBRM's within their operational range for all operational tests except Test 4. During Test 4, the heaters maintained the CBRM's within the heater control band. Generally, the analytical temperatures and test results agreed within 10°F except for a 24°F deviation in one zone which was attributed to a "hot spot" in the flux distribution.

Zone 10/18. Zone 10/18 represents the AWS and contains the pulse-coded modulation radiofrequency (PCM/RF) assembly and the auxiliary storage and playback radio frequency (ASAP/RF) assembly. In the thermal math model, these two components are modeled identically and are subjected to similar environments. Similar theoretical temperatures are predicted for the two components in steady state. An investigation of the power data shows the power dissipation to be identical for the two components. However, in power-on conditions (Runs 4, 6, and 9), there were 20°F differences in similar sides of the PCM/RF and the ASAP/RF. The temperature difference between these two components is unresolved. The transient correlation data show a maximum difference of 4°F between the theoretical and empirical temperatures of the PCM side while a mixiumum temperature difference of 8°F is noted for the ASAP over the 7.75-hr duration of Run 11. This transient data affirm the thermal difference between the two components, although it is less pronounced in Run 11 than in steady state runs.

Zone Pair 11/19. Zone pair 11/19 consists of six rate gyros and five externally mounted components. The external components in this zone have large surface areas that make theoretical and empirical temperature correlations very sensitive to flux simulation and node/measurement comparisons. Overall, the difference between the theoretical and empirical results for the external components is within ±10°F. The rate gyros in this zone correlated within ±6°F for power-on conditions.

The largest steady state temperature deviations (approximately ±20°F in this zone) occurred in the mounting panels. This difference is because of a "fair" node/transducer correlation; a single node representing an area weighted average temperature of the exposed and covered panel being correlated with a transducer that was either exposed or covered. This effect is most pronounced in the component power-on cases where the largest temperature gradients occur.

Zone Pair 12/20. This zone consists of a mounting panel, 15 internally mounted components, a thermal cover, a quarter panel, and two externally mounted components. Steady state correlations agree within ±10°F and most agree within ±5°F. The two externally mounted digital computers have average temperature deviations of ±4°F for both power-on and power-off cases. The zee-bar structure shows agreement within ±5°F for all runs except the cold-case power-on condition, where +15°F differences occurred. To date, this anomoly is unresolved. The only other area of concern in this zone is the high (+10°F) analytical temperatures for the signal conditioning racks. This deviation is attributed to a low theoretical contact conductance between the mounting panel and the components. Transient correlation data for the digital computers exhibit the same correlation under transient conditions (within 4° to 7°F) as they did in steady state. The thermal cover agreement is within 10°F, while the mounting panel is within 1°F.

Zone Pair 14/22. This zone is constructed similar to Zone 12/20. The only differences are the mounting of 22 components instead of 15 on the inside panel and the use of a different insulation cutout pattern on the thermal cover. The two externally mounted components in this zone are CMG inverter assemblies. The CMG inverter assemblies had an average steady state temperature deviation less than 3°F for the power-off conditions. For the power-on conditions, the sides of the CMG inverter assemblies were generally within ±8°F, but the top of the CMG inverter assemblies showed differences as great as 21°F between theoretical and empirical temperatures. These temperature differences indicate that the insulation on top of the CMG inverter assemblies is not adiabatic as modeled. The average temperature deviations for most internally mounted components were less than 4°F and many were less than 2°F. The mounting panel showed similar correlation with no temperature deviation greater than 5°F.

Zone Pair 16/24. Zone 16/24 has 21 components mounted internally and a thermal cover insulation cutout. The external components mounted on the quarter panel in this zone are a CMG inverter assembly 2 and the power transfer distributor. The CMG inverter assembly in this zone had a steady state maximum average temperature deviation less than 9°F. The power transfer distributor compares within 5°F for all steady state runs. However, it was necessary to dissipate the power generated in this component in its base rather than in the top to obtain this match. This indicates that the TMU was improperly constructed and did not simulate the flight component.

The remaining components in this zone generally showed less than a 5°F deviation. These hotter temperatures indicate that a probable error in theoretical contact conductance between the components and the mounting panel exists.

Canister Correlations

Post-test analysis for the canister was performed by using 4 quadrant models, a canister sun end model, a canister TCS model, and an MDA end model. The results obtained from each of the models are described in the following paragraphs.

Quadrants

A compilation of the absolute temperature deviations for the quadrant models is presented in Figure 29. The data show that 83.8 percent of all the canister interior analytical data for Runs 5 and 10 correlated within ±5°F of the corresponding TSU test data. Detailed thermal models of experiment electronic boxes and optical assemblies, not presently included in the analytical models, will increase this percentage significantly. Figures 30 and 31 present a comparison of empirical and theoretical temperatures for pretest and post-test, respectively. This information demonstrates pictorially the effect of using test data to adjust the thermal models during post-test analysis. Figure 31 shows that the deviations between test and analytical temperatures were significantly reduced because of this effort.

For the Quadrant I experiments, the correlation for the HAO is within ±3.0°F for all measurements with the average deviation being 1.0°F. The GSFC average deviation is less than 2.0°F for the entire experiment. The average deviation for the telescope housing tube is 1.5°F.

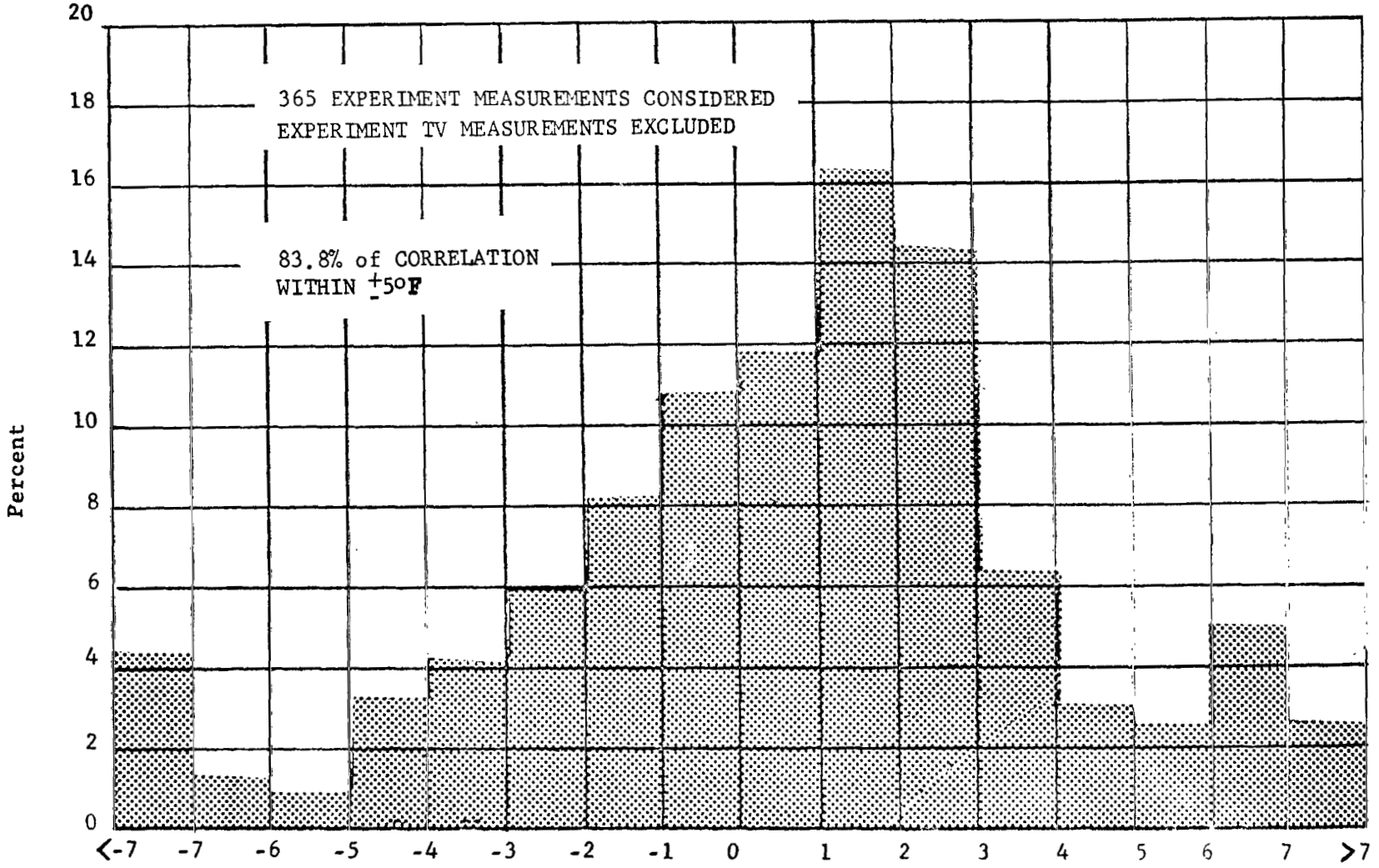

Figure 29. Telescopes correlation results.

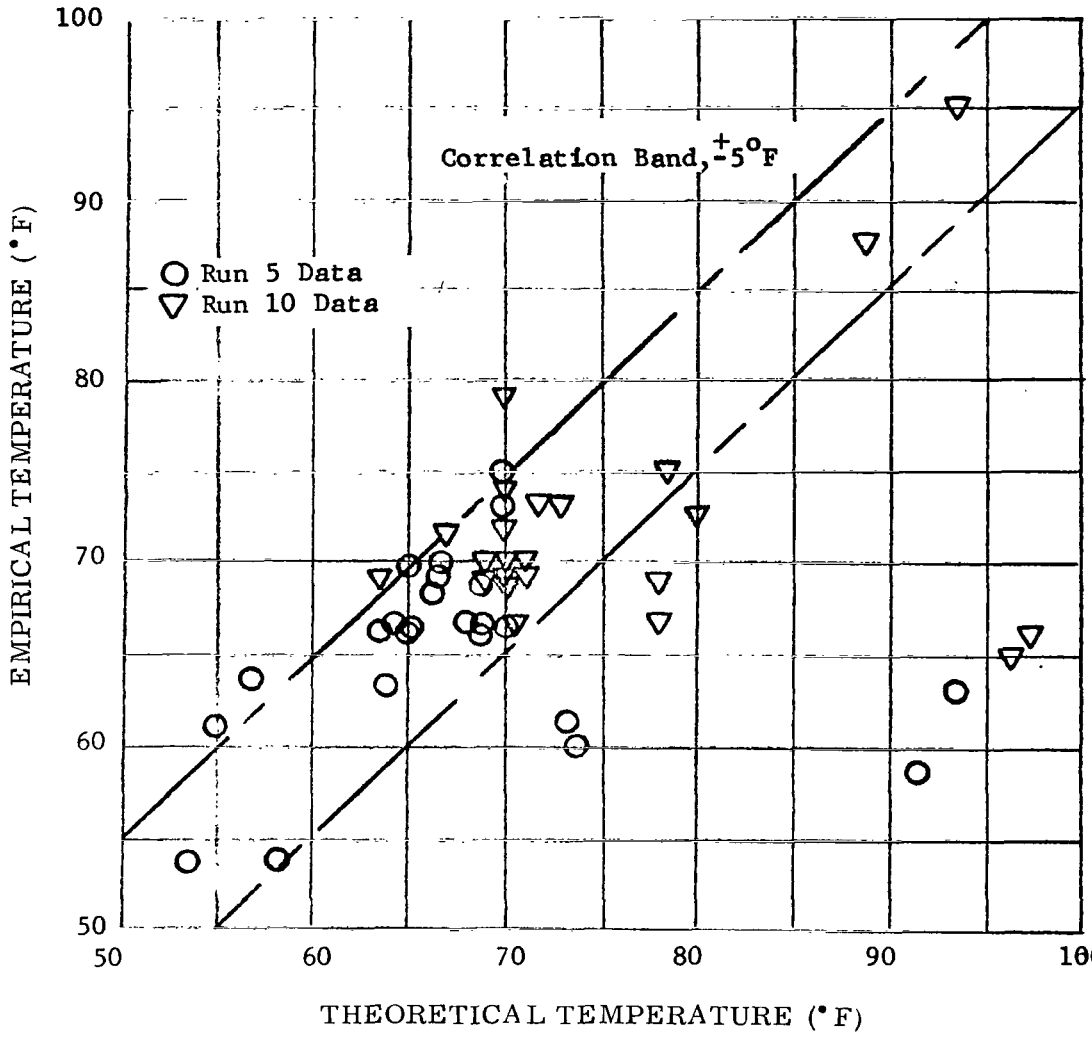

Figure 30. Comparison of telescope empirical temperatures and pretest theoretical temperatures for TSU Runs 5 and 10.

For the Quadrant II experiments (Hα-1 and HCO-A), the Hα-1 telescope assembly correlation is within 4°F except for the heat rejection windows. The consistently lower telescope tube test temperatures indicate degradation of the Hα-1 gold thermal control coating. Measurements indicate that the emissivity of the gold coating varied between 0.10 and 0.15, whereas the analysis assumed an emissivity of 0.05. The HCO-A (S-055) correlation is within ±2.5°F except for the primary mirror and electronic boxes. Because of the lack of modeling details for assembly interiors, good correlation with the corresponding temperature measurements is presently unattainable.

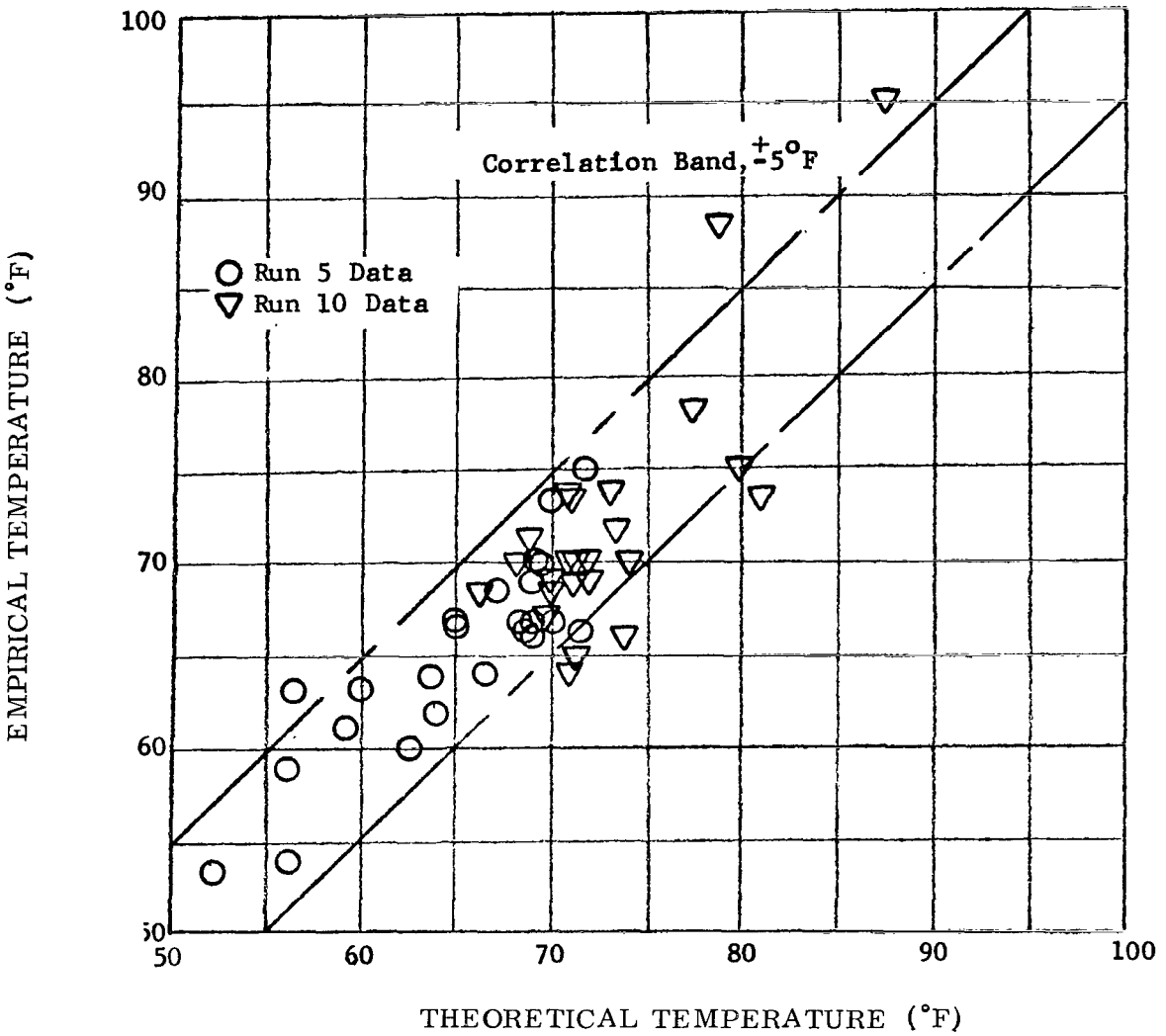

Figure 31. Comparison of telescope empirical temperatures and post-test theoretical temperatures for TSU Runs 5 and 10.

For the Quadrant III experiments (Hα-2 and NRL-B), the Hα-2 model did not correlate well with test data. The analysis assumed that the actual Hα-2 telescope tube emissivity is approximately 0.05 as opposed to the measured value of 0.07. The NRL-B (S-082B) correlation is generally within ±2.5°F. Detailed modeling of the primary mirror assembly and XUV TV camera will improve the correlation.

Correlation for the Quadrant IV experiments (NRL-A and AS&E) shows that the NRL-A temperatures correlate with an average deviation of 2.5°F.

The NRL-A film camera TMU model correlation shows the largest deviation but does not indicate a thermal problem. The average deviation of the AS&E correlation is 0.6°F. The AS&E average experiment temperature exceeds the operational control limits during the extreme hot test (Test Run 10). Two factors contributing to this condition are the apparent rear-housing TCS malfunction and the abnormally high, mirror housing assembly temperature.

Abnormally high temperatures were measured on each of the experiment TV cameras during TSU tests. The analytically determined values represent the average TV case temperatures, whereas the TV thermocouples are internal to the camera and represent the heater temperatures for which thermal models do not exist.

Transient correlation for the experiments was made to verify the experiment's thermal control system modeling and to verify the design of the systems. The boundary conditions used are from the TSU preoperational and activation test data (Tests 11 and 12). The data can be found in Reference 12. Under these conditions, the experiment TCS models are verified by their ability to maintain set-point temperatures on the model heater surfaces with average duty cycles less than 100 percent. Table 3 presents a comparison of the model experiment heater duty cycles with the average duty cycles based on the TSU test, TCS power measurement data for Tests 5, 10, and 12. The average duty cycle is the time-averaged ratio of the experiment TCS power used to the maximum available power. Table 3 shows that the experiment duty cycles are well within limits.

TABLE 3. TELESCOPE HEATER DUTY CYCLES

Telescope	Power Meas.	Duty Cycle (%)					
		Run 5		Run 10		Run 12	
		Model	Test	Model	Test	Model	Test
AS&E (S-054)	NM8030	50	45	30	20	40	40
GSFC (S-056)	NM8032	30	40	7	0	25	--
HCO-A (S-055)	NM8034	70	70	30	20	60	55
NRL-A (S-082A)	NM8040	50	55	20	30	40	55
NRL-B (S-082B)	NM8042	60	65	10	30	40	60
HAO (S-052)	NM8043	70	60	30	30	55	70

Sun End. The boundary conditions for the sun-end model verification were the Test 10 solar flux on the sun end and the canister analytical temperatures. An extreme hot solar constant of 440 Btu/hr-ft^2 was input to the model to simulate the test solar environment. Transient solar flux variations were not considered. Canister sun end nodes were coupled to the canister internally fixed temperature nodes with radiation conductors. In addition, radiation and linear conductors connected the cold plates to the sun end of the canister. The fixed node temperatures from the extreme hot case canister analysis provided the internal boundary conditions for the sun end model.

During the steady state thermal model and test data correlation for the exterior side of the sun end, it was discovered that the analytical temperatures were 25° to 50°F above the thermocouple temperatures. This large temperature deviation was caused by a combination of problems that include: (1) erratic solar flux on the sun end, (2) coating variations, and (3) measurement and model node correlation. Comparison of the interior side measurements with the canister sun end nodes was complicated by the location of two sensors. One sensor was located near the dust shield of the HAO telescope, thereby blocking radiation interchange with the canister cold plates, and the other sensor was covered by a mechanical component. It was decided not to include these measurements in the correlation analysis because of these location problems. To determine the analytical temperature values for test correlation, the sun-end model was run and the results showed that the average central canister sun end interior temperature was 63°F. It was also found that the average peripheral canister sun-end interior temperature was 59.3°F. Averaging these two temperatures results in an analytical canister sun-end plate temperature of 61.1°F which correlates with the 62°F and 61.5°F measured temperatures.

An additional study was conducted with the sun end model to determine the effects of moderate solar flux fluctuations on the canister sun-end interior temperature. It was found that the temperatures of the interior sun end are insensitive to these fluctuations. A reduction in flux from 440 to 400 Btu/hr^2 resulted in a 1°F drop in the canister sun-end interior temperatures while the exterior sun-end temperatures were reduced by 20° to 30°F.

TCS. The TCS model correlations indicated that the average test/analysis deviation (theoretical temperature minus test temperature) for the cold plates was ±0.1°F. Individual predictions for each cold plate were generally within ±1°F for each test.

The radiator test temperatures were always higher than the theoretical results. The high test temperatures resulted from a 10-percent reduction of the effective radiator area that was caused by insulated calibration calorimeter sensors that were mounted in front of the radiator panels. Transient radiator

temperature correlations are 2° to 12°F below the test data. Verification of this reduced area concept was obtained by repeating Test 10 correlation, simulating a 10-percent reduction in effect radiator area. Comparison of Test Run 10 radiator response with the reduced area model results shows that model results were within 5°F of the test data. The average steady-state temperature deviation of the radiator surface temperatures was -2°F for the extreme cold test (Test Run 4).

MDA End Components. None of the MDA end components were found to have exceeded their maximum allowable temperature range during the TSU tests. However, several components were found to be near or below their minimum allowable temperatures during Test Run 3. However, since this mode of operation is not planned for the ATM, these results do not indicate a thermal problem.

During Test Run 3, the MDA end of the canister components that were found to be near or below their minimum storage limits are as follows: Camera control unit Numbers 2, 3, and 6; fine sun sensor control electronics assembly; video switch Number 2; and the synchronous generator. Agreement between the experimental data and the thermal model was within 10°F.

CONCLUSIONS

The successful completion of the ATM TSU thermal vacuum test, in general, demonstrated the adequacy of the ATM thermal design and post-test data analyses verified the vehicle thermal models. More specific conclusion concerning the overall test program are as follows:

1. Several thermal out-of-limit conditions were encountered throughout the test as a result of both design inadequacies and test anomalies.

2. Current mission thermal constraints were verified to be adequate, and no new constraints resulted from the tests.

3. Several components did not reach thermal equilibrium during steady state test runs. This problem indicates one of the difficulties of real-time data evaluation.

4. The value of closed-loop IR environmental simulation was demonstrated.

5. Calibration of the OHS with all test hardware in specified locations is essential because of the background radiation effects that cannot be analytically evaluated.

6. For the OHS, baffled control zones enhance uniformity, reduce all significant overlap, and simplify heat flux control.

7. The overall performance of the solar simulator was poor. Better and less expensive simulation, for thermal purposes, can be achieved with IR simulation.

8. The MSFC test philosophy (described in this report) is a good approach to thermal vacuum testing.

9. Real-time test monitoring by thermal personnel is very highly desirable. Adequate pretest preparation in this area eliminates confusion in actual test operations.

10. Pretest predictions are necessary for timely control of actual test operations.

11. A good knowledge of exact power dissipation rates and locations is essential for good data correlation.

12. To avoid major problems, thermal personnel must be familiar with all test software.

REFERENCES

1. Apollo Telescope Mount Thermal Vacuum Test Plan for Thermal Systems Unit. MSFC 50M74742.

2. ATM Instrumentation Program and Component List (Thermal Systems Unit). MSFC 50M02479.

3. ACE-S/C Operator's Manual, GE/NASA-410-AM-04.

4. Bachtel, F. D.; and Loose, J. D.: Design and Control of an Orbital Heating Simulator. AIAA Paper No. 71-432, AIAA 6th Thermophysics Conference, Tullahoma, Tennessee, April 26, 1971.

5. Final Report, Skylab ATM/TSU Thermal Vacuum Test Operational Checkout Procedures, IR Cage Calibration, T/V Operational/Pre-Operational Test. Quality and Reliability Assurance Laboratory, MSFC.

6. Apollo Telescope Mount Thermal Systems Unit Test Final Report. ED-2002-1174-2, Martin Marietta Corp., Denver, Colorado, January 31, 1971.

7. Analysis of the ATM Thermal Systems Unit Test Data for the MDA End of the Rack and Canister Components and Comparisons of the Test Data to a Thermal Math Model. ASD-ASTN-11607, Teledyne Brown Engineering Co., Huntsville, Alabama, January 26, 1971.

8. ATM Thermal Systems Unit (TSU) Test Thermal Analysis for Components Located in TSU Test Zones 1, 5, and 7. ASD-ASTN-12352, Teledyne Brown Engineering, Co., Huntsville, Alabama, March 15, 1971.

9. Hueter, U.; Connolly, J. M.; and Christensen, P. A.: Apollo Telescope Mount/Thermal Systems Unit - Correlation of Predicted Data and Test Results. AIAA Paper No. 71-433, AIAA 6th Thermophysics Conference, Tullahoma, Tennessee, April 26, 1971.

10. Apollo Telescope Mount Canister Experiment Analysis. ED-2003-1257, Martin Marietta Corp., Denver, Colorado, March 31, 1971.

11. Apollo Telescope Mount TSU Test Data Book. Volume I - Parts 1, 2, and 3, Volume II - Parts 1 and 2, ED-2002-1245, Martin Marietta Corp., Denver, Colorado, January 31, 1971.

REFERENCES (Concluded)

12. Apollo Telescope Mount Experiment TCS Test Results for Thermal Systems Unit Tests. Data Book - Part 2, Martin Marietta Corp., ED-2002-1250, February 1, 1971.

NASA-Langley, 1972 —— 31